Biogeosciences Discuss., https://doi.org/10.5194/bg-2017-310
Manuscript under review for journal Biogeosciences
Discussion started: 24 July 2017

Year-round simulated methane emissions from a permafrost ecosystem in Northeast Siberia

Karel Castro-Morales[1*], Thomas Kleinen[2], Sonja Kaiser[1], Sönke Zaehle[1], Fanny Kittler[1], Min Jung Kwon[1§], Christian Beer[3,4] and Mathias Göckede[1]

[1] Max Planck Institute for Biogeochemistry, Jena, Germany
[2] Max Planck Institute for Meteorology, Hamburg, Germany
[3] Department of Environmental Science and Analytical Chemistry, Stockholm University, Sweden
[4] Bolin Centre for Climate Research, Stockholm University, Stockholm, Sweden

§ Present address: Korea Polar Research Institute, Incheon, Republic of Korea
*Correspondence to: Karel Castro-Morales (kcastro@bgc-jena.mpg.de)

Abstract

Methane emissions to the atmosphere from natural wetlands are estimated to be about 25 % of the total global CH_4 emissions. In the Arctic, these areas are highly vulnerable to the effects of global warming due to atmospheric warming amplification, leading to soil hydrologic changes involving permafrost thaw, formation of deeper active layers, and rising topsoil temperatures. As a result, projected increase in the degradation of permafrost carbon will likely lead to higher CO_2 and CH_4 emissions from these areas. Here we evaluate year-round model-simulated CH_4 emissions to the atmosphere (for 2014 and 2015) from a region of northeastern Siberia in the Russian Far East. Four CH_4 transport pathways are modeled with a revisited version of the process-based JSBACH-methane model: plant-mediated transport, ebullition and molecular diffusion in the presence or absence of snow. This model also simulates the extent of wetlands as the fraction of inundated area in a model grid cell using a TOPMODEL approach, and these are evaluated against a highly resolved wetland product from remote sensing data. The model CH_4 emissions are compared against ground-based CH_4 flux measurements using the eddy covariance technique and flux chambers in the same area of study. The magnitude of the summertime modeled CH_4 emissions is comparable to those from eddy covariance and flux chamber measurements. However, wintertime modeled CH_4 emissions are underestimated by one order of magnitude. The annual CH_4 emissions are dominated by plant-mediated transport (61 %), followed by ebullition (~35 %). Molecular diffusion of CH_4 from the soil into the atmosphere during summer is negligible (0.02 %) compared to the diffusion through the snow during the non-growing season (~4 %). We investigate the relationship between temporal changes in the CH_4 fluxes, soil temperature, and soil moisture content. Our results highlight the heterogeneity in CH_4 emissions at a landscape scale and suggest that further improvements to the representation of large-scale hydrological

Biogeosciences Discuss., https://doi.org/10.5194/bg-2017-310
Manuscript under review for journal Biogeosciences
Discussion started: 24 July 2017

conditions in the model, especially at regional scales in Arctic ecosystems influenced by permafrost thaw, will allow us to arrive at a more process-oriented land surface scheme and better simulate CH_4 emissions under climate change.

Keywords: methane, permafrost, carbon cycle, Arctic, wetlands, winter emissions

1. Introduction

During the last 30 years, atmospheric temperatures at northern high-latitudes have risen more than the global average (Schuur et al., 2015; Serreze et al., 2000). In consequence, many permafrost areas in these regions have experienced expedited thawing rates in recent years. Permafrost in northern high-latitude ecosystems contains twice as much carbon as the current carbon pool in the atmosphere and about half of global soil organic carbon (Hugelius et al., 2014; Tarnocai et al., 2009). About two-thirds of the terrestrial Arctic is classified as wetlands (Liljedahl et al., 2016; Hugelius et al., 2014) and permafrost underlies most of these areas. Wetlands globally contribute about 25 % of the total CH_4 emissions (using bottom-up approaches between 2003-2012) from natural sources into the atmosphere, and from that, nearly 4 % is emitted from wetlands at northern high-latitudes > 60 °N (Saunois and al., 2016). The degradation of freshly available carbon from permafrost thaw is expected to contribute strongly to a positive carbon-climate feedback in Arctic ecosystems (e.g. Beer, 2008). Changes in air temperature, soil topography and projected shifts in precipitation in Arctic tundra ecosystems (Kattsov and Walsh, 2000; Lawrence et al., 2015) influence the soil hydrologic regime in permafrost areas. These changes will therefore also propagate to the magnitude of future emissions of CO_2 and CH_4 into the atmosphere from Arctic terrestrial ecosystems (Hugelius et al., 2014; Lawrence et al., 2015; Schuur et al., 2008). Drier soil columns will enhance methane oxidation and increase CO_2 emissions (Kittler et al., 2016; Kwon et al., 2016; Lawrence et al., 2015; Liljedahl et al., 2016; Sturtevant et al., 2012), also leading to changes in plant community structure (Christensen et al., 2004; Kutzbach et al., 2004; Kwon et al., 2016). Thus, it is imperative to improve our understanding of the effects of climate change in permafrost wetlands, specifically their contribution to greenhouse gases into the atmosphere.

Freeze and thaw soil processes are critical mechanisms that modulate the seasonality of CH_4 emissions in permafrost ecosystems of the Arctic (Panikov and Dedysh, 2000). Most of the annual CH_4 emissions from Arctic wetlands take place during summer (growing season). However, the rising air and soil temperatures during spring promote the melt of snow and ice in the soil, stimulating the microbial production of gas within the active layer (i.e. the surface

soil layer that thaws during summer and freezes again during autumn), which is mostly anoxic. Episodic releases during spring of large amounts of CH_4 in the form of bursts have been evidenced in wetlands (e.g. Friborg et al., 1997; Song et al., 2012), as well as in peatlands (e.g. Tokida et al., 2007) and lakes (e.g. Jammet et al., 2015) of northern high-latitudes. During late autumn, CH_4 emissions still take place when the active layer starts to freeze gradually from the top and ice begins to fill the soil pore spaces, i.e. "zero curtain period". Through this period, the remaining CH_4 in the soil that was produced during the growing season, or in the deeper and still warm soil layers, is squeezed out of the soil. This remaining gas is emitted to the atmosphere via molecular diffusion, and via the "pressure pumping" phenomenon due to advection enhanced by wind (Bowling and Massman, 2011; Massman et al., 1997), through the forming layer of snow (Mastepanov et al., 2008, 2013; Zona et al., 2016). Previous studies have reported that the late autumn CH_4 emissions in Arctic tundra ecosystems account for up to 50 % of the annual CH_4 flux released in the form of gas bursts (Mastepanov et al., 2008; Zona et al., 2016).

Soil and vegetation at northern high-latitudes remain covered by snow during most of the year (October to May). Snow is an effective thermal insulator between the soil and the atmosphere, and it is a porous medium that allows the diffusive exchange of gases. Since there are numerous technical limitations to measuring gas fluxes through the snow during the long cold winter season in the Arctic, a few observational efforts have previously been made to constrain these emissions. These studies have found evidence for the continuation of CH_4 fluxes through snow during the freeze-in period and wintertime in Arctic tundra and permafrost environments. Using flux measurements with chambers and eddy covariance towers, CH_4 emissions have been recorded from snow-covered areas, e.g. in boreal forest soils (Kim et al., 2007; Wahlen and Reeburgh, 1992), boreal peat bogs in Western Siberia (Panikov and Dedysh, 2000; Smagin and Shnyrev, 2015), boreal fens (Rinne et al., 2007), and subalpine soils (Mast et al., 1998; Wickland et al., 1999). Other relevant wintertime studies from Arctic permafrost and wetland areas include the Alaskan tundra (Zona et al., 2016) and in the Zackenberg valley in northern Greenland (Mastepanov et al., 2008; Pirk et al., 2016). In boreal peat bogs of West Siberia, cold season CH_4 emissions contribute from 3.5 to 11 % of the annual CH_4 fluxes (Panikov and Dedysh, 2000). In other Arctic permafrost tundra ecosystems, however, winter CH_4 emissions were one to two orders of magnitude lower than the emissions during summer, and only accumulate in the snowpack in the presence of layers of ice blocking their exit route to the atmosphere (Pirk et al., 2016). Wickland et al. (1999) concluded that in snow-covered subalpine wetland soils, CH_4 fluxes accounted for 25 % of the

annual fluxes. However, the extent to which cold season CH_4 emissions contribute to the annual CH_4 budgets from Arctic wetlands and permafrost ecosystems is largely unknown. Also, projected changes in vegetation phenology due to climate warming in Arctic tundra might also lead to changes in snow cover e.g. more shrubs will tend to hold more snow during winter (Blanc-Betes et al., 2016; Domine et al., 2015). A thicker snow layer will insulate the soil column more during autumn and winter, continuing to contribute to preservation of the heat of the active layer after the preceding growing (zero curtain period) season. This will further impact the extent of subsequent wintertime CH_4 productions and emissions.

In this work, we simulate year-round CH_4 emissions during 2014 and 2015 in a region dominated by low-lying wetland areas and continuous permafrost in the Russian Far East. For this, we use the JSBACH-methane model that includes freeze and thaw soil cycles associated with explicit methane production, transport, and oxidation processes (Kaiser et al., 2017). Although to this day numerical models have made much progress towards better simulating the magnitude and temporal and spatial variability of CH_4 emissions from terrestrial ecosystems, there are still many shortcomings in their parameterizations (Xu et al., 2016). The key schemes of these models are based on traditional theoretical and empirical approaches that describe the mechanistic understanding of the processes involved in the production, oxidation and transport of CH_4 in terrestrial ecosystems (e.g. Grant, 1998; Riley et al., 2011; Walter and Heimann, 2000). Recent developments center on improving the scaling representation from plot to regional and global levels (e.g. Riley et al., 2011; Ringeval et al., 2011; Tagesson et al., 2013; Wania et al., 2010), as well as on improving process-based CH_4 models for regional to global applications (e.g. Bohn et al., 2015; Melton et al., 2013). However, challenges still exist, especially for simulations at regional scales in wetland-dominated areas that are primarily influenced by climate change, such as in Arctic permafrost ecosystems. Models of the emissions of climate-relevant gases in these areas must consider thawing and freezing soil processes (e.g. Schuldt et al., 2013; Zhu et al., 2014), shifts in vegetation coverage (e.g. Chen et al., 2015), and an improved representation of wetlands and water tables (Bohn et al., 2015). Also, most CH_4 models developed at plot scales are not suitable for upscaling to larger areas or for coupling to earth system models (e.g. Mi et al., 2014; Xu et al., 2015). Some recent efforts have been made to model large-scale CH_4 emissions in northern wetland areas related to e.g. soil moisture changes (Lawrence et al., 2015), and for future emissions under climate change (Chen et al., 2015).

The aim of this work is to improve our understanding of year-round CH_4 emissions in an Arctic region dominated by wetlands underlain by permafrost. With this purpose, we simu-

lated CH_4 emissions differentiated among distinct pathways: plant-mediated, ebullition, and diffusion. We improve the JSBACH-model of Kaiser et al. (2017) by explicitly simulating CH_4 emissions to the atmosphere in the presence of snow during the non-growing season, and also provide a revised representation of CH_4 transported by plants that now includes the description of relevant features of vascular plants based on the volume of roots in the soil pore space. We analyze the year-round temporal variation of the CH_4 emissions and their relationship to the environmental drivers at a regional (model domain) scale. The model performance was assessed by comparison of the simulated CH_4 emissions against year-round eddy covariance measurements and summertime chamber flux measurements done in the same area of study. Because temporal variation in the amount of inundated area is are essential for the estimation of CH_4 emissions from wetlands (Prigent et al., 2007), our model also includes a representation of inundated areas using a TOPMODEL approach. We evaluate the modeled horizontal extent of the inundated areas against the wetland area from a high-resolution remote sensing product.

2. Methods

2.1. Site description

The target region of this study is located in Northeast Siberia at the Russian Far East (Republic of Sakha). The model domain is centered on the town of Chersky and is dominated to the west by low-lying wetland areas of the Kolyma River floodplain and to the east by dry upland tundra (Fig. 1a). This region is characterized by the presence of continuous permafrost and active layer depths that range between 20 and 180 cm. The long winter spans from October to May, with daily air temperatures that remain well below the freezing point, while the average daily temperatures are about 13 °C during July (Dutta et al., 2006). Dry climate conditions prevail in this region, with a mean annual precipitation of 218 mm (60 % as snow and 40 % as rain; Dutta et al., 2006). At the Kolyma River floodplain, the soil profile has a top layer of organic material (~15 cm) that is located above alluvial mineral soils, i.e. silty loam (Kittler et al., 2016; Kwon et al., 2016). In this area, the vegetation is heterogeneous and representative of wet tussock tundra. There, the water-logged areas are covered by the tussock-forming sedges, such as *Carex appendiculata* and *Carex lugens*, and cotton grasses like *Eriophorium angunstifolium* (Kwon et al., 2016). During the spring snowmelt (May and June), large sections of the Kolyma floodplain usually become inundated, and during summer, the extent of surface water recedes due to evapotranspiration and drainage to the river channels located nearby. However, most areas remain inundated throughout the year (Kwon et al., 2016). The eastern part of the model domain has more elevated slopes and drier soils with

Biogeosciences Discuss., https://doi.org/10.5194/bg-2017-310
Manuscript under review for journal Biogeosciences
Discussion started: 24 July 2017

tundra vegetation dominated by grasslands and forests, i.e. dwarf evergreen and deciduous shrubs, *Sphagnum* mosses, and lichens, but few trees (Dutta et al., 2006; Merbold et al., 2009). Loess soil deposits originating from the accumulation of aeolian and alluvial sediments characterize the soil in this region.

2.2. Model configuration

The model results presented in this work were obtained with a regional configuration in offline mode of the land-surface component of the MPI-ESM (Max Planck Institute for Meteorology Earth System Model), the so-called Jena Scheme Biosphere Atmosphere Coupling in Hamburg (JSBACH) model. We used a JSBACH version that has been extended from the version of the CMIP5 activity (e.g. Brovkin et al., 2013; e.g. Raddatz et al., 2007; Reick et al., 2013). Modifications include the addition of a multilayer hydrology scheme (Hagemann and Stacke, 2015) and the representation of permafrost physical processes (Ekici et al., 2014). The model domain covers an area of 7 degrees in longitude (158° E to 165° E) and 3 degrees in latitude (66.5° N to 69.5° N). Using a horizontal resolution of 0.5° (Fig. 1b), this results in a model domain with 14×6 equally spaced grid cells. The vertical structure in the model domain comprises 11 non-equidistant soil layers with thicknesses that increase from 6.5 cm at the top to 23.2 m at the bottom, reaching a maximum column depth of 40.5 m. In the model domain, the root zone is confined to the top five layers (maximum depth of 1.1 m) with maximum and mean root depths of 0.88 m and 0.42 m respectively. The soil ice content is restricted to the top six layers (maximum depth of 2.0 m), with bedrock located from the 6th layer downwards.

A prescribed fraction of each grid cell is used to discriminate between hospitable and inhospitable land (Reick et al., 2013). The hospitable part is then subdivided into a maximum of 11 tiles each of which is assigned a land cover type to represent the sub-grid scale heterogeneity of vegetation cover. These tiles may have different sizes. In our model domain, only four land cover types were present (ordered by dominance in the model domain): 1) C3 grasses, 2) Deciduous trees, 3) Evergreen trees and 4) Deciduous shrubs (see Fig. S1 for their spatial distribution in the model domain).

The model configuration contains the basic JSBACH modules with components from the Biosphere-Energy-Transfer-Hydrology model, BETHY (Knorr, 2000). The vegetation carbon is categorized into three groups: wood, green, and reserve. The soil carbon and decomposition model Yasso07 (Tuomi et al., 2009, 2011) takes care of the transport and decomposition of carbon into the soil. It simulates the breakdown of litter and soil organic matter based on measurements of soil carbon and litter bag experiments, and has been previously implement-

ed into JSBACH (Goll et al., 2015; Thum et al., 2011). In Yasso07, soil litter is divided into three classes: non-woody, woody, and humus. The non-woody class is subdivided into four pools representing groups of chemical compounds with an independent decomposition rate determined by changes in air temperature and precipitation, thus it has no relation to plant species (Goll et al., 2015; Tuomi et al., 2009).

Most of the CH_4 emissions into the atmosphere from Arctic terrestrial ecosystems are from wetland areas, thus the representation of the wetland extent in CH_4 models is of relevance. In this model, the standard soil hydrology scheme (Hagemann and Stacke, 2015) was extended to 11 vertical layers to resolve a grid cell mean water table position. This is determined by the saturation state of the soil layers: the lowest soil layer that is not completely frozen or completely saturated contains the grid cell mean water table, with the exact location within the layer given as the layer fraction that is saturated. The position of the mean water table in the grid cell is used in a TOPMODEL (TOPographic MODEL) approach (Beven and Kirkby, 1979; Kleinen et al., 2012; Stocker et al., 2014) to define the fraction of the grid cell with a water table at or above the soil surface. With the implementation of this hydrological scheme, JSBACH now has a dynamic wetland module that allows modeling the water table and the fractional area of inundation at a grid cell scale (Kleinen et al., 2012). The main input parameter for TOPMODEL is the so-called compound topographic index, CTI (Kirkby, 1975). CTI represents a topographic profile that is used to define how likely a landscape point is to become water saturated and is defined as $\gamma_i = \ln(\alpha_i / \tan \beta_i)$, where α_i is a dimensionless index used to determine the source contributing area at point i, and $\tan \beta_i$ is the local slope. Based on statistical information of the CTI, areas in a landscape with similar CTI values will have similar hydrological responses allowing a simplification of the hydrological calculations in the model. In this work, the CTI values were generated from the CEH-UK high-resolution global dataset of topographic index values (Marthews et al., 2015). The distribution of CTI values within a model grid cell was estimated with gamma function approximation (Sivapalan et al., 1987). The position of the local water table depth (z_i) in the TOPMODEL scheme is calculated as:

$$z_i = \bar{z} + \frac{1}{f}(\chi_i - \bar{\chi}) \quad (1)$$

where $\bar{z}$ is the grid cell mean water table, χ_i is the local CTI index, $\bar{\chi}$ is the grid cell mean CTI index, and f is the exponential decay of transmissivity with depth and sets the dependence of flooding on water table variation. With the explicit inclusion of the TOPMODEL approach into JSBACH, the inundated fraction of the grid cell is simulated with z_i located at or

above the surface. Consequently, the grid cell wetland area is defined where $0 \leq z_i$, and it is subject to a minimum CTI threshold value χ_{min_cti} defined to limit the maximum possible areas that can be flooded following the approach of Stocker et al. (2014), with lower values leading to larger areas. In this configuration, the constant prescribed χ_{min_cti} and f are tunable parameters of the TOPMODEL module used to expand or reduce the fraction of inundated surface areas in a model grid cell. Within the inundated fraction of the grid cell, a constant relative soil moisture saturation of 0.95 is assumed. The decomposition of soil organic matter is reduced to 35 % of the aerobic decomposition in line with Wania et al. (2010).

The CH_4 production and emission processes in the model are tightly linked to the volumetric soil porosity to allocate gas transport (Kaiser et al., 2017). This model configuration contains a permafrost module to explicitly simulate soil freeze and thaw processes coupled to the hydrological and thermal regimes in the soil column (Ekici et al., 2014). This is a relevant process in permafrost regions where changes in the soil ice content drive the seasonal changes in the volumetric soil pore space, and changes in the soil moisture ultimately determine whether the soil pores are filled with water or air.

2.2.1. Methane module

In this work, the JSBACH-methane configuration presented in Kaiser et al. (2017) underwent several modifications. Besides being coupled to TOPMODEL and the soil carbon Yasso07 components, the CH_4 module itself acquired several extensions: i) a refined description of plant-mediated transport, ii) allowance of gas transport via diffusion through the snow during the non-growing season, and iii) change in the order of transport processes. Details on each of these changes are listed in Appendix A.

In the process-based JSBACH-methane module, the equilibrium between the concentrations in free atmosphere, soil air, and soil moisture is assumed for the initialization of the methane and oxygen concentrations in the soil. During each model time step, CH_4 is produced in the soil column depending on the soil hydrological conditions (i.e. ice content and soil moisture), soil temperatures, soil pore space, and the available decomposed carbon. The fraction of CH_4 produced from the total carbon decomposition under anaerobic conditions for mineral soils ($f_{CH4anox}$) is prescribed as 0.5 (i.e. 50 % of the anaerobically decomposed carbon is used to produce CH_4). Since this setting is highly uncertain, the model response to a range of $f_{CH4anox}$ values is tested in sensitivity experiments as part of this work.

Two explicitly modeled CH_4 oxidation processes are contained in the JSBACH-methane module: bulk soil oxidation and rhizospheric oxidation of methane (plant oxidation). These

oxidation pathways interact iteratively in the model with the methane transport processes, reducing the methane pool when oxidation takes place.

To facilitate the interaction between the CH_4 and TOPMODEL modules, in this new model version the ice-free pores of the soil column are saturated to 95 % with moisture to justify the accumulation of water at or above the soil surface depending on the topographic profile. However, the soil temperatures, ice content and available carbon for CH_4 production are not influenced during this process. Thus, CH_4 emissions from a grid cell happen under a combination of soil temperatures, ice content, and available carbon decomposition characteristic of an unsaturated soil column on the one hand, and ice-free soil pores with soil moisture at 95 % saturation on the other. Ultimately, the methane production, oxidation, and transport processes only take place in the saturated portion of the grid cell (see schematic in Fig. S2). The transport of the gases to and from the atmosphere is distributed across four explicitly modeled transport processes: plant-mediated transport, ebullition, and molecular diffusion without snow and through the snow. The efficiency of each transport process is based upon prevailing soil moisture content (which is set to constant 95 % saturation in the inundated areas) and takes into account the ice-corrected volumetric soil porosity, which in turn depends on the soil temperature.

The *plant-mediated transport* in the model only takes place in areas with C3 grasses and follows Fick's first law, including the diffusion of gas between the plant aerenchyma system and the surrounding soil pore spaces. In wetland ecosystems, many plants have developed an efficient aerenchyma system that functions as a transport mechanism of gases between the atmosphere and their roots. Plants need oxygen for metabolic processes and the root exodermis is an efficient barrier that keeps the oxygen inside the plant roots and, at the same time, slows down the diffusion of gas from the soil into the roots; thus, the gas flow is restricted by the thickness of the exodermis tissue. In the JSBACH-methane module, the root exodermis has a prescribed diffusivity value of 80 % of the total diffusivity of the same gas in water, for the gas between the plant and the surrounding soil pores. In combination with a shallow root zone and few gas transporting roots therein, in the original JSBACH-methane model, plant-mediated transport was the slowest emission process and therefore took place only after ebullition and molecular diffusion. For the configuration of this work this condition was modified (see Appendix A for further details). *Ebullition* takes place when excess gas that has not been dissolved in the available soil pore liquid water forms bubbles that are rapidly transported upwards from their source in the deep soil layers through the water into the atmosphere, successfully bypassing the oxic areas in the soil. *Diffusion* is the molecular transfer of gas from

high to low concentration gradients between soil layers and the atmosphere following Fick's second law, and in this model version, it is now also allowed to take place through a layer of snow. The latter is a simplified formulation that does not take into account the enhanced advection of gas in the snowpack due to wind, i.e. pressure pumping.

Between the model time steps, the gas amounts are constant, whereas the gas concentrations change in relation to the varying ice-free pore space. The detailed description of how these processes and transport pathways are modeled in JSBACH-methane can be found in Kaiser et al. (2017).

2.2.2. Experimental set up and sensitivity experiments

The model was forced with daily reanalysis atmospheric data CRUNCEPv7 (The Climate Research Unit from University of East Anglia, analysis of the National Centers for Environmental Prediction reanalysis atmospheric forcing version 7.0) from 1901-2015 with a spatial resolution of 0.5° (Viovy and Ciais, 2016). Prescribed annual means of atmospheric CO_2 values were also used to drive the model (https://www.esrl.noaa.gov/gmd/ccgg/trends/global.html). The model was spun-up for 10,000 years of simulation by repeating cycles of atmospheric data from 1901-1930 (~330 cycles) to equilibrate the soil carbon pools. Among other modules, the methane module was deactivated during this procedure. After that, simulations were initialized with reanalysis data from 1931 until 2015 (85 years). To allow equilibration of the soil carbon pools to the hydrology as well as equilibration of CH_4, a model adjustment period of 850 years (10 cycles using the 85 years of reanalysis data) was added. After this, the output of the 11th cycle was stored and used for subsequent data analysis. In this simulation, we used prescribed reference values for parameters in the TOPMODEL and methane modules that represent the control simulation. A description of the most relevant prescribed parameters and variables in the control simulation is outlined in Table 1.

To evaluate the robustness of the model, a set of sensitivity experiments was done to test six selected parameters whose value is prescribed and are involved in the newly modified parts of the code for this model version: the simulation of inundated areas (TOPMODEL module), diffusion of methane through plants and snow, and the allocation of soil carbon under anaerobic conditions for methane production. The selected parameters are: χ_{min_cti} for the evaluation of TOPMODEL, d_r and R_{fr} for the evaluation of plant-mediated transport, h_{snow} and ϕ for evaluation of the transport via diffusion through the snow, and the fraction of anoxic decomposed carbon that becomes CH_4 ($f_{CH4anox}$) for the evaluation of the methane production. For

each parameter, reference values from the control simulation were decreased or increased by a fixed value (shown together with the results in Table 2), resulting in a total of 12 independent sensitivity simulations.

Specifically, the selected values for ϕ and $f_{CH4anox}$ were kept within ranges of previously reported values in the literature, whereas for the other four parameters tested we chose extreme values with respect to the defined values in the control simulation. Each sensitivity simulation consisted of a re-initialization from the conditions in the control simulation from the last time step on 31 December 1999. This was to allow the model to adjust to the parameter change for 13 years before the year of result analysis (i.e. 2014). In order to keep consistency in the treatment of our simulations, the same re-initialization procedure was done for a reference simulation by re-initializing the control simulation from the restart conditions on 31 Dec 1999, as in the sensitivity experiments, but without changing any parameter (i.e. maintaining the same parameters as in the control simulation). The results from the sensitivity experiments were compared to the results from the reference simulation. The temporal resolution of all the model simulations is 30 min, with hourly output averaged for analysis into daily and monthly values.

2.3. Observational data

2.3.1. Wetland product

Methane emissions to the atmosphere in the model occur largely from areas with a water table at or above the surface. These fractions of "inundated" areas in each model grid cell represent the horizontal extent of wetlands, including lakes, peatlands, or temporally inundated areas. As described in Section 2.2, in our study this inundated fraction is estimated through the TOPMODEL approach for each grid cell. To evaluate the performance of TOPMODEL in our model configuration, we compared the spatial distribution of the inundated areas per grid cell to the wetland extent remote sensing product from ENVISAT ASAR (European Space Agency's ENVISAT with an Advanced Synthetic Aperture Radar operating in Wide Swath mode C-band). The ENVISAT ASAR WS-wetland product (EAWS) was tested for operational monitoring in northern Russia, where small-scale ponds and an overall high soil moisture level are common surface features (Reschke et al., 2012). The backscatter of the EAWS product for high latitudes has a higher spatial and temporal resolution (150 m and 2 to 3 days, respectively) than other commonly used wetland products (e.g. Prigent et al., 2007), which have spatial resolutions of the order of kilometers. Thus, the EAWS product is able to capture small water bodies like tundra ponds and wetland patches that remain almost un-

changed throughout the year and are associated with permafrost areas. This product has been previously evaluated against other land cover and wetland products. The spatial coverage of the EAWS product includes most of northern Russia and is subdivided into 10 mosaics, each with different coverage areas. It is freely available as GeoTIFF images, each representing a 10-days-mean in a wetland map during July and August in 2007 (i.e. 01-10 July, 11-20 July, 21-31 July, 01-10-August, 11-20 August, 21-31 August, all in 2007; Reschke et al., 2012).

For the evaluation of the modeled wetland extent, each 10-days-mean image of the EAWS product was mapped to the same grid of georeferenced rectangular cells in our JSBACH domain. From the total 84 model grid cells, 35 model grid cells fall into the area coverage of the EAWS images (Fig. 1b). The wetland fraction from the EAWS remote sensing product (w_{rs}) in percentage was calculated as the ratio of pixels flagged as wetland (ID = 1) to the total number of pixels contained in the grid cell. In the model, the spatial wetland fraction (w_{mod}) is represented as the fraction of the total grid cell area that is inundated (i.e. with a water table at or above the soil surface). To facilitate a direct comparison against w_{rs}, the w_{mod} values from the control simulation were averaged to the same 10-days-mean in 2007 as the remote sensing data.

2.3.2. Chamber measurements

To evaluate the performance of the methane model, we compared the total modeled methane fluxes (F_{mod}) to the total methane fluxes measured with flux chambers (F_{ch}) in the Kolyma River floodplain (Fig. 1b, see also Kwon et al., 2016). In this study, chamber fluxes from an undisturbed control area were considered for model evaluation purposes. The chamber flux measurements were done during the early to mid-growing season (15 June to 20 August) in 2014. As additional ancillary variables, water table depth, vegetation cover, and soil temperature were also measured. For further details on the gas measurements, calculations, and discussion of the chamber flux results the reader is referred to Kwon et al. (2016).

The surface area of each chamber along the control transect is about 0.36 m^2, therefore even all 10 chambers combined can only represent a very small fraction of the surface area of a single model grid cell (2.5 x 10^9 m^2). However, since both F_{mod} and F_{ch} are normalized to a unit area ($CH_4/m^2/day$), it is possible to directly compare F_{ch} to F_{mod}. For the model evaluation exercise, we extracted the daily F_{mod} corresponding to the same dates of the chambers flux measurements, and only the emissions from that model grid cell where the chamber plots were geographically positioned (grid cell A, Fig. 1b). We also show the results from an adjacent grid cell (grid cell B, Fig. 1b) to demonstrate the spatial heterogeneity between the model grid cells for a region close to the chamber flux measurements.

Biogeosciences Discuss., https://doi.org/10.5194/bg-2017-310
Manuscript under review for journal Biogeosciences
Discussion started: 24 July 2017

Due to the heterogeneous topographic characteristics in the study site, the microsites of the chamber plots within the control area include water-saturated (average water table during the growing season > 10 cm below the surface, observed in 8 chamber plots) and unsaturated characteristics (dry soil conditions, i.e. water table < 10 cm below the surface, observed in 2 chamber plots, Kwon et al., 2016). Thus, the total F_{ch} from the chamber plots was averaged separately for the wet plots (F_{ch_wet}) and for the dry plots (F_{ch_dry}). This heterogeneity in the data finds its equivalent in the model grid cell heterogeneity as estimated by TOPMODEL, where on average only a portion of the grid cell area is inundated and the rest remains dry during a specific period of time. Thus, to obtain the total F_{ch} the chamber flux measurements F_{ch_wet} and F_{ch_dry} were scaled to the daily-inundated fractions w_{mod} for the selected model grid cell g:

$$F_{ch} = F_{ch\_wet} \cdot w_{mod} + F_{ch\_dry} \cdot (1 - w_{mod}) \quad (8)$$

At two of the chamber sites, temperature sensors (hereinafter referred to as redox systems) continuously recorded the soil temperature profile at three soil depths (4, 16, and 64 cm). The redox systems are located in a site dominated by dry soils and a site dominated by wet soils, and thus these temperature measurements reflect the important influence of soil water levels on the soil thermal regime across the seasons.

2.3.3. Eddy covariance measurements

The model results were also compared to ecosystem-scale methane fluxes measured by an eddy covariance tower situated in the Chersky floodplain. This tower is located at 68.62° N and 161.35° E, near the north end of the chamber plot transect in the control area (Tower 2 in Fig. 1 of Kittler et al., 2016) and has an instrument height of 5.11 m at an elevation of 6 m a.s.l. The data are available at 30 min intervals. For details on the instrumental setup, raw data collection, and eddy covariance data post-processing, the reader is referred to Kittler et al. (2016). The field of view ("footpring area") of an eddy-covariance system with the given sensor height above the ground normally extends up to several hundred meters in the main wind direction at any given time (see e.g. Fig. 1 of Kittler et al., 2016, for an example of a footprint). The position of the eddy covariance tower falls within the area of model grid cell A (shown in Fig. 1b) and far away from the grid cell borders; thus, all the CH_4 emissions measured with the eddy covariance system fall within the area of grid cell A.

3. Results

3.1. Evaluation of inundated areas

Within the context of this analysis, inundation fractions are given as the percentage of the total grid cell area that holds water at or above the surface. The first comparison between remote sensing (w_{rs}) and simulated (w_{mod}) wetland extents, based on the original TOPMODEL configuration, showed that the model mostly overestimated the extent of inundated fractions. For example, in the predominantly wet sections north of the model domain (> 68.5° N), the averaged w_{rs} is 9 % whereas w_{mod} was simulated at 15 %. However, in drier areas (< 68.5° N) w_{rs} is on average 1.2 % whereas the model did not predict inundation in those grid cells. Since modeled methane emissions only take place in the inundated areas of a grid cell, it was necessary to modify the prescribed TOPMODEL parameters to improve w_{mod}. To achieve this, the initially prescribed maximum threshold for inundation (χ_{min_cti}) was modified so that the horizontal extent of inundated areas in the model decreased compared to the results of the initial configuration. Changes in this value have an effect only on wet areas. In Fig. 2 the latitudinal distribution of the percent difference between w_{mod} and w_{rs} for 01-10 August 2007 for the selected value of χ_{min_cti} (i.e. 12) is depicted. We show only the results corresponding to one EAWS image because the results are similar for the other five available GeoTIFF images. The distribution of modeled grid cell inundated areas during the same period of time is shown in the inset of Fig. 2: model grid cells with more than 1 % of inundated area are found from the northwest to the southeast part of the model domain, and also include some grid cells in the western and northern parts. The spatial distribution of the modeled inundated areas throughout the year does not vary considerably since the inundated fraction in the model takes into account the accumulation of liquid and frozen water. However, the fraction of inundation within each grid cell varies in relation to drier or wetter conditions. After parameter adjustment, the comparison between w_{mod} and w_{rs} resulted in a mean difference of −1±8 % and a median of 2 % integrated over all the six 10-days-mean periods. However, some outlier values result in considerable single-pixel differences between w_{mod} and w_{rs}, ranging from +19 % in the southernmost areas (< 68.5° N) to −23 % in the northernmost areas (> 69° N). The best agreement between model and EAWS product is observed between latitudes 68.5° and 69° N (Fig. 2).

During the process of optimization between w_{mod} and w_{rs}, the parameter f was not modified because a change of this parameter would influence both the inundated and dry areas of a grid cell. The chosen value for χ_{min_cti} that resulted in a closer agreement between w_{mod} and w_{rs} is used in the configuration for the control and reference simulations in this work. We ex-

emplify the effect on the modeled methane emissions due to changes in the χ_{min_cti} value, and include this parameter in the sensitivity experiments of section 3.2.

3.2. Sensitivity experiments

To investigate the impact of different values of selected model parameters (shown in column two of Table 2) on the individual processes and total CH_4 emissions, we compared the results from the reference simulation at daily resolution in 2014 to six pairs of sensitivity experiments (Fig. 3, with pairs of sensitivity experiments shown as panels within rows a through f). The annual mean model domain CH_4 emissions for each experiment are also summarized in Table 2. From all the sensitivity experiments, a significant difference in model output between the reference simulation and the simulations with modified settings was found only for parameters χ_{min_cti} and $f_{CH4anox}$ (for both variables n=365 and $p<0.01$ after a nonparametric Wilcoxon rank-sum test; see also Fig. 3, all panels in row a and f).

The predefined threshold parameter χ_{min_cti} in the TOPMODEL module sets the maximum possible area in the grid cell that can be flooded. A higher χ_{min_cti} value leads to a larger wetland extent in already inundated areas within the model grid cell. Consequently, our results show that a change in χ_{min_cti} has a large effect on the CH_4 emissions: describing $\chi_{min\_cti} = 13$ leads to nearly 1.5 times higher CH_4 emissions during summer and autumn compared to the results using the reference value of 12, and about two times higher than the results with the lower χ_{min_cti} test value of 11 (Fig. 3, row a). The effect of varying χ_{min_cti} in the resulting model mean inundated fraction is shown in Fig. S3 of the supplementary material. With the higher χ_{min_cti} value (i.e. 13), the annual average of the inundated fraction in the model domain (0.054) increases by 54 %, whereas with the lower χ_{min_cti} value (i.e. 11) the annual average inundated fraction in the model domain (0.024) decreases by 35 %, both with respect to the annual average of the inundated fraction in the model domain from the reference simulation (0.0367).

The $f_{CH4anox}$ parameter is a prescribed fixed value used to define the fraction from the total decomposed soil organic matter that will be allocated for CH_4 production (i.e. anoxic carbon mineralization), with the rest becoming CO_2. In our model configuration, this is considered for mineral soils only. A value of $f_{CH4anox} = 1.0$ would mean that all of the decomposed soil carbon would become CH_4 under anaerobic conditions. The value used in the reference simulation is 0.5. In the context of the sensitivity study, we tested the effect on the simulated CH_4 emissions by decreasing $f_{CH4anox}$ to 0.1 (i.e. 10 % of the decomposed carbon will become CH_4, whereas 90 % will be oxidized), and to 0.3 (i.e. 30 % of the decomposed carbon will

become CH_4 whereas 70 % will be oxidized). The resulting mean CH_4 emissions in the model domain responded evidently to changes in the value of $f_{CH4anox}$: with the largest $f_{CH4anox}$ value of 0.5, the summer CH_4 emissions were five times higher than the summer emissions with the lower $f_{CH4anox}$ value of 0.1 (Fig. 3, row f).

The remaining parameters tested within this sensitivity study (Table 2) show that with the chosen values, the simulated CH_4 emissions are not significantly different from each other. The d_r parameter associated with the plant-mediated transport pathway shows that the difference between the simulated CH_4 emissions is not statistically significant through the year between fine plant roots of 2 mm (as defined in the reference simulation) and thicker roots of 8 mm (Fig. 3, row b). A small variation can be noted for ebullition and diffusion mostly during July (Fig. 3, column 1 and 2 of row b). The difference in emissions due to an increase in the soil root volume from 20 % to 60 % is also not statistically significant (Fig. 3, row c).

For the selected parameters associated with the emissions of CH_4 through the snow, the porosity of snow $\phi = 0.64$ used in the reference simulation corresponds to a ρ_{snow} of 330 kg/m^3, characteristic of wind packed snow, and a mean tortuosity $\tau = 0.77$, calculated with Eq. 6. We tested two other values of ϕ, and by doing so simulated the properties of other types of snow: $\phi = 0.71$ corresponds to a settled snow type with ρ_{snow} of 263 kg/m^3, and $\phi = 0.86$ corresponding to fresh damp new snow with a lower ρ_{snow} of 128 kg/m^3 (both ϕ values were calculated with ρ_{ice} = 910 kg/m^3). The tortuosity value also decreases with denser snow, thus the corresponding τ values are 0.79 and 0.85 for aged and fresh snow, respectively. Our sensitivity results from these experiments show that the differences between the winter CH_4 emissions through a layer of fresh damp snow, or through a wind packed snow layer, are not statistically significant (Fig. 3, row d).

Finally, the fixed limiting snow depth, which discriminates between ordinary CH_4 transport via diffusion and diffusion through the snow, was also tested. In the reference simulation, this switch happens at a fixed $h_{snow} \geq 5$ cm. In the sensitivity experiments, we decreased h_{snow} to 3 and 1 cm. Our results show that the differences between the individual and total CH_4 emissions through various h_{snow} values are not statistically significant (Fig. 3, row e). Visually however, an effect is seen in the CH_4 emissions from mid-October until mid-November (Fig. 3, column 4 of row e), with the emissions through snow taking place earlier in time and being of a larger magnitude if h_{snow} is thinner. Nevertheless, this shift in the CH_4 emissions through the snow is not observed in the total CH_4 emissions. The regionally aggregated CH_4 transport via ebullition, diffusion and plants during the same months is reduced as h_{snow} becomes thin-

ner, thus compensating for the shift in the emissions in the presence of snow and maintaining a mass balance in the annual total emissions.

3.3. Evaluation of modeled emissions with eddy covariance and chamber measurements

3.3.1. Evaluation of year-round modeled total CH_4 emissions

To evaluate the model performance, we compared the modeled CH_4 emissions at grid cell scale to measurements from eddy covariance and chambers. Methane emissions from eddy covariance measurements are available from April 2014 until September 2015, while data from chamber measurements are restricted to the period of June to August 2014. The modeled total CH_4 emissions used for this comparison correspond to the grid cell where both the eddy covariance tower and the chambers are geographically located (grid cell A, Fig. 1b). Also, we show the modeled total CH_4 emissions from the neighboring grid cell to the west (grid cell B, Fig. 1b) and further show their association with environmental variables and prescribed parameters in the model (section 3.3.4).

Considering the large spatial scale of the modeled emissions, the monthly mean of the CH_4 emissions from the eddy covariance and chamber measurements agree well with the monthly model results for the grid cells A and B and for 2014 and 2015. Positive correlations between the measured and modeled CH_4 fluxes, with correlation coefficients (R^2) higher than 0.95, are observed in all comparisons except for the correlation between the chamber measurements and the results from grid cell B (R^2=0.85; Fig. 4). Fig.5a and b display box plots of the monthly mean CH_4 emissions for summer months only (June, July, and August) from each data set: both grid cells (A and B), eddy covariance data for 2014 and 2015, and chamber flux measurements for 2014 only. In 2014, the median of the CH_4 emissions from grid cell B is consistently higher than the rest of the other compared datasets, and this is followed by the eddy covariance fluxes (Fig. 5a). The same is observed in 2015 (except for the lack of chamber flux measurements during that year; Fig. 5b). During both years, the median of the modeled CH_4 emissions from grid cell A is generally lower than the rest of the compared data sets (Fig. 5a and b).

The time series of the monthly mean CH_4 emissions from the model grid cell A and B is compared with the observational datasets in Fig. 5c. The shaded area around the mean values is one standard deviation calculated from the daily values; thus, it represents the range of variability in the emissions within each month. Compared to the eddy covariance measurements, the model underestimates the CH_4 emissions in grid cell A, but the modeled values from grid cell B are higher for most of 2014 and 2015 (Fig. 5c). Averaged over both years, results from

grid cell A are lower than the results from the eddy covariance measurements by 4.7±8.1 mg CH_4 m^{-2} d^{-1}. In contrast, CH_4 emissions from grid cell B are on average larger than the eddy covariance measurements by as much as 6.1±10.5 mg CH_4 m^{-2} d^{-1}. During winter, the model CH_4 emissions from both grid cells are on average 3.7 mg CH_4 m^{-2} d^{-1} lower than the eddy covariance measurements (Fig. 5c). The modeled CH_4 emissions from both grid cells show large interannual variability; however, the interannual variability of the observations is even larger than the model data.

Methane emissions from the chamber flux measurements are lower than the model results of both grid cells for June and July 2014 (on average by 16.6 mg CH_4 m^{-2} d^{-1} in June and 24.3 mg CH_4 m^{-2} d^{-1} in July), but also than the eddy covariance flux data (on average 15.3 mg CH_4 m^{-2} d^{-1} and 25.1 mg CH_4 m^{-2} d^{-1} in June and July, respectively). However, the results from grid cell A are in closer agreement with the chamber flux measurements, with the chamber data showing larger emissions by 8.2 mg CH_4 m^{-2} d^{-1} compared to results from grid cell A during August 2014 (Fig. 5c).

Despite the disagreement between mean values from the model and observations from eddy covariance and chamber fluxes, there is an overlap in the monthly variability between all data sets during 2014 as depicted by the shaded areas. It is furthermore important to note that the monthly range of values in the eddy covariance data, particularly during July, August, and September, has a large spread, denoting that daily variability in these data exceeds that of the model results. A larger disagreement is observed during the summer of 2015 between results from grid cell B and the eddy covariance data. However, the daily variability of CH_4 emissions from grid cell A falls well within the range of values from eddy covariance measurements in the summer of 2015 (Fig. 5c).

3.3.2. Relationship between soil temperatures and CH_4 emissions

To examine the relationship between soil temperatures and CH_4 emissions, we first compared the modeled and measured soil temperature profiles. The temporal evolution of the vertical profiles of daily soil temperatures, measured with the redox systems, is shown in Fig. 6a for the wet plot and in Fig. 6b for the dry plot in 2015. The measured soil temperatures were only available from August to December in 2014, and behaved similarly in 2015 for the same months; thus we show here only the vertical profiles for 2015. To construct the soil temperature profiles, the temperature values measured with the sensors at 4, 16, and 64 cm depth were linearly interpolated every 2 cm through the vertical soil column. For comparison, the modeled vertical profiles of the daily soil temperatures in 2015 for the top four soil layers (bottom depth of 3, 12, 29, and 58 cm) in grid cells A and B were also linearly interpolated

every 2 cm (Fig. 6c and d). During winter and spring, the measured soil temperatures are not lower than −16 °C, while the modeled temperature values are as low as −26 °C within extended sections of the period from December to May in both 2014 and 2015. The measured values in the dry plot show abrupt temperature changes during the transition between freezing conditions (< 0 °C) and warmer conditions (> 0 °C) during mid-December and mid-May. This abrupt change is also seen in the wet plots with freezing conditions remaining for a shorter period of time; i.e. the change to and from warmer temperatures takes place only from the end of January until mid-May. Also, generally colder temperatures are observed in the top part of the soil column and gradually extend to deeper soil layers as the season progresses. In contrast, although the modeled soil temperatures reach lower values during winter, a smoother transition of temperature is evidenced from freezing to warmer conditions in spring, and to freezing conditions again in autumn. In the model results, the soil temperature remains homogeneous along the vertical profile.

Measured temperatures above freezing conditions occur from mid-June until the end of September. As summer progresses, warmer soil temperatures extend from the surface to deeper soil layers (Fig. 6a and b). In the dry plot, however, the warmer conditions remain only in the top 16 cm of the soil column (Fig. 6b) due to lower soil moisture content and lower thermal conductivity compared to the wet plot. The model is able to capture the timing of the seasonal transition from spring to summer at the end of May, the duration of the summer conditions, and the magnitude of the temperature values. For grid cells A and B, the summer temperature profiles are more similar to the wet than to the dry plot. The average measured soil temperature in the range of the sensor's depths (top 64 cm) during summer (June, July, and August, 2015) in the dry plot was 2.1 °C, while in the wet plot for the same period the average measured soil temperature was 4.7 °C; in the model, the average soil temperature in the top 58 cm is about 4.9 °C during summer of 2015. The modeled warm soil temperatures (> 5 °C) reach deeper soil layers in summer; however, this is not observed in the measured data. This could simply be due to the vertical resolution between the sensors of the redox systems, with a large gap between 16 and 64 cm depth. Thus, to evaluate the deeper extent of the warm soil temperatures depicted in the model, this portion of the soil column needs to be better resolved vertically by the measurements.

A larger disagreement between measured and modeled soil temperatures, however, occurs during the transition from autumn to winter. The measured temperatures remain around −3 °C in the top 64 cm from October to mid-December, until they change abruptly to around < −10 °C in the dry plot during mid December (Fig. 6b), and in the wet plot towards the end of

January (Fig. 6a). In contrast, the model results show a gradual transition between the seasons, with decreasing soil temperatures to values < 0 °C starting in mid-October (Fig. 6c and d).

To investigate the effect that the abrupt changes in the measured soil temperatures have on the CH_4 emissions, we plotted the soil temperature at 12 cm (for model data) and at 16 cm (average measured values for the wet and dry plot) against the total CH_4 emissions for grid cells A and B and from eddy covariance measurements in 2014 (Fig. 7). The modeled soil temperatures represent the entire grid cell conditions, whereas the CH_4 emissions are only from the saturated and inundated portion of the grid cell (Fig. S2). Despite this disagreement, CH_4 processes in the model follow the seasonal variation in soil temperature. This relationship, however, is only possible to analyze on a qualitative basis. A positive non-linear correlation between soil temperatures and CH_4 emissions is observed in all comparisons. Fitted polynomial curves are plotted on top of each data set. During 2015 (and 2014, data not shown), the CH_4 emissions measured with eddy covariance drop faster with the changes of temperature until freezing conditions. Below 0 °C, constant CH_4 emissions are observed despite the further decrease in soil temperature. In contrast, the change of modeled CH_4 emissions with respect to changes in soil temperature is more gradual, especially from autumn to winter in both years, until few methane emissions take place in winter associated with lower soil temperatures than the ones registered by the sensors in the redox systems. The lower simulated soil temperatures in the model might explain the lower CH_4 emissions during winter and spring compared to the eddy covariance data.

3.3.3. Winter emissions

In Fig. 8, we show the CH_4 emissions through the snow from the eddy covariance measurements and those simulated by the JSBACH model, both at daily resolution. The time series of daily emissions are shown from the beginning of October 2014 to the end of April 2015 (Fig. 8a) and in October 2015 (Fig. 8c). The difference between the model methane emissions for grid cells A and B, and eddy covariance data is shown in Fig. 8b and d for the same cold season periods. Comparable to the eddy covariance measurements, the winter emissions in the model drop abruptly at the end of October 2014, remaining low until March 2015. During October 2014, the model CH_4 emissions in grid cell B are higher, while the emissions from grid cell A are more similar to the eddy covariance measurements (Fig. 8a). This is also found in the first half of October 2015 (Fig. 8c). However, during this month the eddy covariance measurements show no clear trend, while the model data shows a decreasing trend over time in CH_4 emissions. During most of the winter in 2014/2015 (i.e. from November 2014

until April 2015), the modeled CH_4 emissions from grid cells A and B remain lower than the eddy covariance measurements by on average 2.8 mg CH_4 m^{-2} d^{-1}. During January, February and March in 2015 the mean model CH_4 emissions for grid cells A and B are 0.4 mg CH_4 m^{-2} d^{-1}, while the eddy covariance data show persistently higher values with 3.8 mg CH_4 m^{-2} d^{-1} for the same months (Fig. 8a). Model emissions start rising (2.0 mg CH_4 m^{-2} d^{-1}) to values similar to those in the eddy covariance data (2.8 mg CH_4 m^{-2} d^{-1}) only in mid-April.

To investigate if the CH_4 emissions from the model during the entire wintertime are equivalent to the total winter emissions measured by eddy covariance, we calculated the cumulative sum of the modeled CH_4 emissions and eddy covariance from October 2014 to March 2015. Our results show that, despite a higher earlier release of methane in e.g. grid cell A, the modeled total emissions released during that winter are not equivalent to those from the eddy covariance measurements, with the latter providing evidence for larger total CH_4 emissions in winter than predicted by the model (Fig. 8e). In our model, the emissions through the snowpack take only into account the molecular diffusion of gas, whereas the advection of gas due to wind as an additional transport pathway is not included.

3.3.4. Model spatial heterogeneity

Environmental characteristics are important drivers for the temporal variability of the CH_4 emissions. Contrasting differences in the input parameters for grid cells A and B are responsible for differences in the modeled physical conditions, which in turn lead to the differences in the CH_4 emissions between these neighboring model grid cells. Because the relative differences between the total CH_4 emissions from grid cell A and B are similar in 2014 and in 2015, we show only the comparison of environmental characteristics for 2014. The cover fraction of the plant functional types in the model domain (Fig. S1), as well as the soil (bedrock) and the maximum depth of the root zone (Fig. S4a and b), are all input parameters prescribed for each model grid cell. The soil depth ranges between 0.1 to 10.6 m, and the depth of the root zone from 0.1 to 0.89 m. Grid cell A has a prescribed shallower soil column (0.89 m) and 5 cm deeper root zone (0.72 m) than grid cell B (10.6 m and 0.67 m, respectively). Furthermore, grid cell A has lower soil moisture and soil ice content relative to the pore volume in the top five soil layers, and larger inundated area, compared to grid cell B (Fig. 9a, b, and d). A considerable difference between grid cells A and B is in their cover fractions of C3 grasses, with 33.3 % in grid cell A compared to 91.6 % in grid cell B. This difference has direct influence on the CH_4 emissions through the plant roots. As shown in Figs. 9e and f, the largest plant-mediated CH_4 emissions at the peak of the growing season in grid cell B (103 mg CH_4 m^{-2} d^{-1}) exceed those in grid cell A (28 mg CH_4 m^{-2} d^{-1}) by a factor of three. Conse-

quently, the dominant pathways for methane emissions during summer for grid cell A are ebullition and diffusion, which in combination are four times as large as in grid cell B for the same transport pathways (Fig. 9e and f).

3.4. Year-round modeled methane emissions

Domain means of the seasonal courses of CH_4 emissions from the different CH_4 transport pathways in 2014 and 2015 from the reference simulation, as well as the daily mean snow depth, are shown in Fig. 10. The results show a distinct seasonality for each of the individual methane emission pathways. Overall, the lowest CH_4 emissions occur between November and May. During these months, the timing of the CH_4 emissions through the snow is largely modulated by the variability of the snow depth, and accordingly, takes place predominantly in spring and autumn. The methane emissions via plants, ordinary molecular diffusion, and ebullition are mostly restricted to the period May through mid-November in areas when and where h_{snow} does not exceed 5 cm (or it is simply absent). The magnitude of the CH_4 emissions through molecular diffusion is the least relevant among the four modeled transport pathways.

3.4.1. Summertime CH_4 transport pathways

From May to mid-November, CH_4 emissions take place only in the grid cells with inundated areas, with the highest flux rates simulated for the center west of the domain (Fig. 11). During this period h_{snow} is either absent or does not exceed 5 cm. Ebullition precedes the emissions through plants during late March 2014 and during early April 2015. In both years, the mean of the CH_4 emissions in the model domain through ebullition rise steadily, reaching up to 5 mg CH_4 m^{-2} d^{-1} by mid June. Following a short but pronounced decrease to 3.5 mg CH_4 m^{-2} d^{-1}, the ebullition of CH_4 rises again to reach its maximum during mid summer with similar magnitude in both years (7.2 mg CH_4 m^{-2} d^{-1}). However, this maximum is achieved later in 2014 (9^{th} of August) than in 2015 (16^{th} of July). After its maximum in 2014, ebullition of gas steadily decreases from mid-August until mid-November, while in 2015 the emissions via ebullition remain high during most of July and start to decrease steadily only in August, leveling up during the first part of September and after that continuing to decrease until mid-November (Fig. 10). The gas transported through ebullition contributed 33.9 % in 2014 and 35.7 % in 2015 to the total annual CH_4 emissions. Annually, CH_4 transported by plants is the dominant pathway, contributing 61 % of the total domain mean annual CH_4 emissions. These emissions take place from May to mid-November in areas where $h_{snow} < 5$ cm, and are restricted to areas where C3 grasses are present (Fig. S1 and panels of the first column in Fig. 11). The domain means of the CH_4 emissions through plants reached their maximum by 5^{th}

August in 2014 and by 16th July in 2015 with a maximum value of 15 mg CH_4 m^{-2} d^{-1} in both years (Fig. 10).

Methane emissions through ordinary molecular diffusion also take place if $h_{snow} < 5$ cm in the inundated portion of the grid cells (panels in the third column of Fig. 11). In the absence of snow during summer and early autumn, CH_4 emissions via diffusion in the model domain average about $2.9x10^{-3}$ mg CH_4 m^{-2} d^{-1} (similar in 2014 and 2015), while during late autumn, winter and early spring the emissions via this pathway are only possible if $h_{snow} \geq 5$ cm. For those few grid cells with $h_{snow} < 5$ cm during the non-growing season (November to May), the CH_4 emitted via molecular diffusion is two to three orders of magnitude lower (mean of $3.4x10^{-5}$ mg CH_4 m^{-2} d^{-1} for both years) than during the growing season (June to September). Methane transported via molecular diffusion during the growing season contributes only 0.02 % to the total CH_4 annual budget.

3.4.2. Impact of snow on the seasonal distribution of CH_4 emissions

During early spring, late autumn and winter, methane emissions take place through a layer of snow ≥5 cm deep. The mean maximum accumulation of snow in the model domain takes place in spring: earlier in 2014 (0.23 m on 21st March) than in 2015 (0.17 m on 8th March). The spatial distribution of the spring snow depths in 2014 and 2015 (Fig. S4c and d) show deeper snow layers in the dryer southwestern part of the model domain. On average, the layer of snow starts to melt rapidly at the beginning of May in 2014 and at the end of April in 2015, reaching total snowmelt by 2nd June 2014 and 27th May 2015 (Fig. 12a). The average CH_4 emissions through the snow in the entire model domain during January and February are 0.17 mg CH_4 m^{-2} d^{-1} in 2014 and 0.12 mg CH_4 m^{-2} d^{-1} in 2015 (Fig. 10 and Fig. 12g). The CH_4 emissions fluctuate through the winter (Fig. 12g), and these changes are related to changes the thickness of the snow cover (Fig. 12a). During the rapid snowmelt period in spring (March, April and May), the daily domain average CH_4 emissions to the atmosphere through the snow increase (Fig. 10) with domain mean average spring CH_4 emissions of 0.65 CH_4 mg m^{-2} d^{-1} and 0.43 mg CH_4 m^{-2} d^{-1} in 2014 and 2015, respectively. The maximum domain mean daily emissions of CH_4 outside the growing season are modeled during May, with 1.66 mg CH_4 m^{-2} d^{-1} in 2014 and 0.96 mg CH_4 m^{-2} d^{-1} in 2015 (Fig. 12g), and these take place predominantly in the central part of the model domain (panels in the fourth column of Fig. 11). In the entire model domain, the emissions of CH_4 through snow contribute 4.7 % and 2.7 % to the total mean annual CH_4 emissions for 2014 and 2015, respectively. Although deeper spring snow layers are modeled in 2014 than in spring 2015 (Fig. 12a) in the areas where CH_4 is emitted to the atmosphere (Fig. S4c and d), the total methane emissions through snow

from January to mid-May amount to ~70 mg CH_4 m^{-2} in 2014, and only 66 % of that value in 2015 (~46 mg CH_4 m^{-2}; Fig. 10).

Integrated over the model domain during autumn, the snow starts to accumulate later in 2014 (9^{th} October 2014) than in 2015 (30^{th} September 2015), and the snow layer becomes rapidly deeper until December at a similar accumulation rate for both years (Fig. 12a). As the snow accumulates, the emissions via ebullition and plants decline, but diffusion through snow rises as soon as the snow depth reaches 5 cm in some grid cells. From November to December, the mean CH_4 emissions through the snow in the domain amount to 37.3 mg CH_4 m^{-2} in 2014, and 33 % less in 2015 (12.4 mg CH_4 m^{-2}). The modeled CH_4 emissions through the snow only consider the ordinary molecular diffusion of CH_4 between the soil and the atmosphere, and the pressure pumping effects due to advection of gas by wind is not taken into account.

3.4.3. Impact of environmental controls on CH_4 flux seasonality

Several systematic interannual differences between the timing and magnitude of the individual CH_4 transport pathways in 2014 and 2015 were found in the model results. These include e.g. the maxima of the individual emissions, which occur a few days later in 2014 than in 2015. To improve the interpretation of the temporal variability of CH_4 emissions through the different pathways, we analyze the temporal changes in soil temperatures within the root zone (top five soil layers) as simulated by the model. It is important to note that because of the current structure of the model, the depicted soil temperature in Fig. 12b reflects the average conditions of the entire grid cell, and not only the inundated portion with saturated soils where CH_4 emissions take place. Still, the analysis of the temporal changes in the mean grid cell soil temperatures gives an indication of the nature and magnitude of the seasonal changes that indirectly control the CH_4 emissions. The gradient of temperatures in the root zone for the entire domain between spring and summer is steeper in 2015 than in 2014 (Fig. 12b). The maximum soil temperatures are similar in both years (8.7 °C); however, this maximum was reached at the beginning of August in 2014 while in 2015 the maximum was reached at the beginning of July and remained high throughout August. During the rest of the year, the mean soil temperatures were 2 °C higher in 2014 compared to 2015 (−4.5 °C and −6.5 °C, respectively). The mean changes in temperature in the top five soil layers reflect the changes in the air temperature as given in the atmospheric forcing data. According to the mean air temperature in the model domain, the summer of 2014 was colder than the summer of 2015 (by up to 10 °C for individual days during June, Fig. S5a). This leads to delayed warming of the soil, later high CH_4 production, and thus a later release of CH_4 into the atmosphere during summer in 2014 than in 2015, as shown in Fig. 12h.

Biogeosciences Discuss., https://doi.org/10.5194/bg-2017-310
Manuscript under review for journal Biogeosciences
Discussion started: 24 July 2017

Figure 12c depicts the model domain mean relative soil moisture content in the top five soil layers for 2014 and 2015. As with soil temperature, the soil moisture reflects the average conditions of the entire grid cell and not just those in the inundated portion where the soil moisture is set to nearly saturation levels. Although these values are not linked to the area of the grid cell where CH_4 is transported and emitted, we can still show the temporal changes of soil moisture content in the non-saturated portion of the grid cell between years and seasons. These changes can be linked to changes in precipitation patterns (Fig. S5b) and soil temperatures. According to the mean precipitation from the CRU-NCEP reanalysis data, more precipitation fell in the model domain during early July in 2014 compared to the same period in 2015 (Fig. S5b). This led to the top five soil layers becoming wetter on average in 2014 (Fig. 12c) and potentially allowed higher thermal capacity in the soil during that period. In contrast, more precipitation fell during most of August and September 2015 than for the same periods in 2014 (Fig. S5b), leading to an increase in the relative moisture content during most of the end of summer and early autumn in 2015 (Fig. 12c). These changes in soil moisture influence the soil temperature at the grid cell scale, and thus the soil temperature feedbacks to the CH_4 processes. Therefore, it is possible to indirectly relate the effects of changes in grid cell scale soil moisture to the changes in the modeled CH_4 emissions.

The mean relative soil ice content in the top five layers of the model domain (Fig. 12d) was higher in winter and spring of 2014 than in 2015, and this is a general observation for the entire domain. However, the air temperatures from the reanalysis data during that period were on average higher in 2014 than in 2015 (Fig. S5a). The ice content decreases at a fast rate during June in both years, however the complete loss of ice in the soil is reached earlier in June of 2015 than in 2014, and this is a reflection of colder temperatures in June 2014, delaying the complete melt of the more abundant ice in the soil during that year relative to the same month in 2015 (Fig. S5a). The soil ice content feeds back to the modeled available pore space for CH_4 production, thus the ice content changes in the soil can be indirectly linked to the CH_4 emissions. The earlier reduction of ice content in the soil during June 2015 might have contributed to the earlier release of methane during that month, via ebullition, compared to 2014 (Fig. 12f). The lower air and soil temperatures at the beginning of autumn in 2015 (Fig. S5a) led to higher ice content in the soil during October 2015 compared to 2014 (Fig. 12d). The soil temperatures remain warmer in autumn of 2014, enabling more CH_4 to be emitted during November 2014 when the snow starts to accumulate in contrast to 2015 (Fig. 12g and h).

Biogeosciences Discuss., https://doi.org/10.5194/bg-2017-310
Manuscript under review for journal Biogeosciences
Discussion started: 24 July 2017

4. Discussion

4.1. Sensitivity experiments

Our sensitivity experiments show that changes in the values of most of the selected parameters result in no significant differences in the modeled CH_4 emissions for the individual pathways or the total flux. Specifically, varying the diameter of roots from finer to thicker, and varying the amount of available soil volume occupied by roots, did not cause significant differences in modeled CH_4 emissions.

Using three different values for root diameter also caused no significant differences in the total CH_4 emissions with the new formulation of the plant transport in the JSBACH-methane model. These results suggest that the revisited and simplified formulation for plant-mediated transport of gas allows a reduction in the uncertainties of methane transported through this pathway, which previously relied on predefined plant root characteristics that are often not available from observational studies. Instead, we define the volume in the soil that is occupied by roots.

The lack of sensitivity of the CH_4 emissions to most of the selected parameters might ultimately be due to the explicit restriction of gas transport via diffusive processes modeled by Fick's first law (plant transport and molecular diffusion through snow) that was set in the model. The role of this restriction is to limit the diffusion of gas once the concentration gradient between two interfaces equals zero i.e. it reaches equilibrium. Thus, this restriction takes place when the concentration gradient between e.g. the gas in the soil pore spaces and within the plant's roots (for plant-mediated transport) or between the gas in the soil pore spaces and the atmosphere above the snow layer (for diffusion of gas trough the snow), equals zero. Because the transport pathways can occur in parallel (except for diffusion with and without a snow layer), or emissions can be shifted in time, the modeled total CH_4 emissions may not be influenced by the set of parameters tested here. Changes in the threshold depth of snow that limit the diffusion of gas through this layer revealed some differences in the partitioning of the methane flux into the four transport pathways. These differences indicate that a thinner threshold depth favors the other three transport pathways. However, the resulting total CH_4 emissions with the three tested snow threshold depths were not statistically different.

Changes to the values of the parameters χ_{min_cti} and $f_{CH4anox}$ caused statistically significant differences in the total CH_4 emissions ($p<0.001$). A significant increase in CH_4 emissions with increasing inundated surface area (TOPMODEL parameter χ_{min_cti}) highlights the importance of this approach to regulate the extent of the grid cell inundated areas. However, further in-

vestigations and improvements in the TOPMODEL approach, as well as a better integration into the hydrology scheme of JSBACH, are needed in order to better constrain the modeled CH_4 emissions with JSBACH.

Finally, the model showed also a large sensitivity to changes in the parameter values of the fraction of anaerobic decomposed soil organic matter that becomes methane, $f_{CH4anox}$. In soil systems where fermentation and methanogenesis are exclusive processes, i.e. without the presence of alternative pathways for respiration via terminal electron acceptors by other microbial groups that ultimately can suppress the production of CH_4, the CO_2:CH_4 ratio after anaerobic carbon mineralization is normally 1:1 (Conrad, 1999), i.e. $f_{CH4anox} = 0.5$. We used this value in the reference simulation because it was previously reported in the literature as characteristic of water-saturated polygon centers (Preuss et al., 2013), and it is similar to the value reported for unsaturated zones in boreal bogs (Wahlen and Reeburgh, 2000). However, in wetland areas, CH_4 is still subject to oxidation after its production and the CO_2:CH_4 ratio is expected to increase and to vary among types of wetlands (Bridgham et al., 2013). Thus, although the value of $f_{CH4anox}$ determines the fraction of CH_4 produced under anoxic conditions, this CH_4 still can undergo oxidation before it is emitted to the atmosphere. Furthermore, $f_{CH4anox}$ can be theoretically related to the fraction of CH_4 that is left after oxidation and before it is emitted to the atmosphere ($f_{ox} = 1 - f_{CH4anox\_left}$). Values of f_{ox} have been previously reported as ranging between 0.6-0.7 for sites with vascular plants. On the other hand, it can be nearly equal to 1 in sites with, for example, a layer of *Sphagnum* moss, where the majority of the produced CH_4 is oxidized, or in bottom soils in pond centers where slow molecular diffusion of CH_4 takes place through the water (Knoblauch et al., 2016). Under the latter conditions, f_{ox} can be approximated to > 0.9 (i.e. > 90 % of the produced CH_4 is oxidized before it is emitted to the atmosphere). This value has been estimated in polygonal ponds without vascular plants, empirically supporting the relevance of CH_4 oxidation below the water table in these types of environments (Knoblauch et al., 2016). A lower CH_4 oxidation fraction occurs in the presence of vascular plants that are effective at bypassing the aerobic areas in the soil. Under these conditions, $f_{CH4anox\_left}$ can increase moderately from 0.2 to 0.4 (i.e. f_{ox} is from 0.6 to 0.8, meaning that 60 to 80 % of the produced CH_4 is oxidized in the soil column). The results of our sensitivity experiments provided evidence that the magnitude of the simulated CH_4 emissions responds strongly to the value of $f_{CH4anox}$. Although current estimates for $f_{CH4anox\_left}$ from laboratory and on-site experiments are still scarce, they mostly agree that those are lower than our reference value of 0.5. This is expected because $f_{CH4anox\_left}$ excludes the portion of CH_4 that is oxidized directly after production, whereas $f_{CH4anox}$ is only the ini-

tially produced CH_4. Still, our modeled CH_4 emissions might benefit from prescribing a spatially variable $f_{CH4anox}$ value linked to the distribution of vascular plants and soil wetness in the model domain.

4.2. Year-round model methane emissions

We simulated for the first time year-round methane emissions in a Northeast Siberian region centered on the city of Chersky, including emissions during the non-growing season. Our results showcase the ability of the improved JSBACH-methane model to reproduce seasonality in the CH_4 emissions when compared to fluxes measured by eddy covariance and chambers in a study site near Chersky. During the growing season, plant-mediated transport dominated the emissions, contributing about 61.4 % in 2014 and 61.7 % in 2015 of the total annual CH_4 emissions, followed by ebullition (33.9 % and 35.7 %) and molecular diffusion during summer when snow is not hindering the emissions (0.02 % for both years). These patterns agree with the findings presented in Kwon et al. (2016) for the CH_4 emissions measured with chambers at the Chersky floodplain, and by Kutzbach et al. (2004) and Knoblauch et al. (2016) in the Lena River Delta, who found evidence that in the presence of vascular plants, the dominant CH_4 transport pathway in these wetland ecosystems is diffusion through the aerenchyma structures of the plants. Methane emissions during the non-growing season contributed 4.7 % and 2.7 % of the annual methane emissions in 2014 and 2015, respectively.

The JSBACH-methane model does not explicitly consider some mechanisms related to the carbon decomposition and thaw in Arctic permafrost and wetland ecosystems, such as: CH_4 production in the soil from root exudates (Knoblauch et al., 2016; Ström et al., 2012), vertical transfer of carbon and its vertically resolved decomposition (Braakhekke et al., 2011, 2013 and 2014; Koven et al., 2015), and microbial community dynamics (McCalley et al., 2014) involved in anoxic CH_4 oxidation or the production of CH_4 in anaerobic microsites confined in oxic soils. Although these processes might contribute substantially to the dynamics of CH_4, research on these processes in soil-permafrost and wetland environments is still lacking or poorly understood with controversial results so far (Bridgham et al., 2013).

At the grid cell scale, we observed that the heterogeneity in the prescribed input parameters in the model domain, such as the initial soil depth, ultimately control the variability of the modeled environmental characteristics. The contrasting coverage of C3 grasses in two neighboring model grid cells predominantly explains the shift in the dominant CH_4 transport pathways and seasonal changes.

Our results show a good agreement between the modeled CH_4 emissions (at the grid cell scale) and measured CH_4 emissions with eddy covariance and chambers. Overall, the mod-

eled year-round and measured methane emissions at daily temporal resolution are in the same order of magnitude, and both fall within their monthly range of variability. In the model, CH_4 emissions integrated in our study region were on average 22.5 mg CH_4 m^{-2} d^{-1} during the growing season of 2014 and 2015. These modeled values are also in good agreement with measurements in other Arctic wetland areas influenced by permafrost using eddy towers, chambers, and more recently with airborne techniques. Kutzbach et al., (2004) reported CH_4 emissions of 28 mg CH_4 m^{-2} d^{-1} measured with chambers during the onset of the growing season from a polygon center of the wet tundra in the Lena Delta. For a variety of locations in polygons of the Lena Delta, Sachs et al. (2010) reported mean summer methane emissions of about 55 mg CH_4 m^{-2} d^{-1}, and for the same study site, Knoblauch et al. (2016) presented mean summer fluxes of 46 mg CH_4 m^{-2} d^{-1} also measured with chambers at the margins of ponds. Larger summer methane emission values have been reported elsewhere, e.g. from automatic chambers at the Zackenberg research station, with maximum emissions of about 168 mg CH_4 m^{-2} d^{-1} at the onset of the growing season (Mastepanov et al., 2008). Merbold et al. (2009) reported CH_4 emissions of ~600 mg CH_4 m^{-2} d^{-1} measured by chambers at the peak of the growing season (August) in 2005 in the Chersky floodplain.

At the lower end of the observational data, Wille et al. (2008) measured CH_4 emissions of about 30 mg CH_4 m^{-2} d^{-1} during mid-summer also in the Lena Delta. The authors argued that the measured values were generally lower than other estimates and that the main controlling factors of their measurements were low soil temperatures and the influence of atmospheric turbulence during their period of study. Rinne et al. (2007) reported CH_4 fluxes of about 84 mg CH_4 m^{-2} d^{-1} measured using eddy covariance at a boreal fen in southern Finland. Eddy covariance CH_4 fluxes measured in the Alaskan tundra showed a larger range of values, with an average of 32 mg CH_4 m^{-2} d^{-1} during the onset of the growing season (Zona et al., 2016). Finally, airborne measurements of CH_4 emissions from wetlands in Alaska were estimated to be about 56 mg CH_4 m^{-2} d^{-1} (Chang et al., 2014).

4.3. Representation of inundated fractions of the grid cell

In this model version, we incorporated the TOPMODEL approach to explicitly model the distribution of inundated areas according to the topography profile. Although this is still only a robust approximation, the implementation of this approach improved the ability of the model to represent wetlands the highly heterogeneous landscape of northeastern Siberia. Furthermore, this was a considerable improvement to alleviate restrictions associated with the traditional hydrology scheme of JSBACH, which does not allow modeling of grid cells with standing water (Kaiser et al., 2017; Hagemann and Stacke, 2015).

Biogeosciences Discuss., https://doi.org/10.5194/bg-2017-310
Manuscript under review for journal Biogeosciences
Discussion started: 24 July 2017

In the model, the fraction of the grid cell that becomes inundated refers to the area where the water table lies at or above the soil surface. In nature, most wetlands have periods of the year when no visible standing water is above the surface, and the water table can sometimes lie just below the surface (Bridgham et al., 2013; Kwon et al., 2016). Previous works have demonstrated the dependence of CH_4 emissions on the location of the water table in tundra ecosystems (e.g. Kwon et al., 2016; Merbold et al., 2009; Sturtevant et al., 2012). The work by Kwon et al. (2016) revealed that CH_4 fluxes measured by chambers in the Chersky flood-plain are significantly influenced by the location of the water table at the plot scale, with larger CH_4 emissions in sites where the water table was at or above the surface compared to drier sites. However, although CH_4 oxidation predominantly exceeds production in dry sites, low CH_4 fluxes during the growing season were measured in areas where the water table was located below the soil surface. Further improvements in the model are needed to better simulate CH_4 emissions in non-inundated areas, as discussed below.

4.4. Impact of the revised model structure

The model reproduces well the observed temporal trends in the CH_4 emissions, and patterns can be linked to changes in the environmental controls. However, as a result of introducing the TOPMODEL approach to allow the representation of inundated areas, , the connection among the soil characteristics of the inundated part of the grid cell has been compromised in this model version. Namely, the soil moisture content is no longer connected to the soil ice content and to the soil temperature. Still, in this model version the soil ice content controls the pore space available for CH_4 transport, and the soil temperature influences, among other variables, the carbon decomposition rates. However, a direct connection between each of these physical variables and the CH_4 processes is definitively present. These physical drivers influence the heat capacity of the soil and the ice content (i.e. soil freeze and thaw processes), and control the accumulation of gas, microbial activity, diffusion rates of gases, and the amount of oxygen in the soil (Sturtevant et al., 2012; Wickland et al., 1999; Pirk et al., 2016). Between data years, the soil temperature in summer of 2014 was lower from mid-June than at the same period during 2015, leading to a phase lag in the maximum summer CH_4 emissions of nearly a month earlier in 2015. However, during the autumn of 2015, the soil was colder than in 2014, with more soil ice content and less methane production during this period of the year. This translates into lower CH_4 emissions to the atmosphere from November 2015 until the end of the year than during the same period in 2014. Because seasonal changes in soil wetness must be taken into account for modeling year-round gas emissions in permafrost Arctic tundra environments (Pirk et al., 2016), the JSBACH-methane version used for this

work requires further improvements to better integrate the TOPMODEL approach into the grid cell thermal and hydrology schemes.

4.5. Simulation of grid cell soil temperature

Large uncertainties in the simulation of CH_4 emissions from northern wetlands with models come from the poor representation of freezing and thawing soil processes (Ekici et al., 2014), snow layer dynamics for the emission of gas during the cold season, and the robust mapping of the distribution of wetlands (Bridgham et al., 2013). Kaiser et al., (2017) reported that the process-based JSBACH-methane module considers the effects of permafrost thawing and freezing, thus the seasonal changes of the physical state of the soil, on the CH_4 processes. However, our analysis of the soil temperature profiles showed that during the cold season the simulated soil temperatures are nearly 10 °C lower than the values measured on site. Moreover, they gradually increase through spring and summer to reach values similar to the measurements. In contrast, the soil temperature profiles measured in the Chersky floodplain display a pronounced seasonal cycle linked to the thawing and freezing processes in the soil (Göckede et al., 2017). These differences are related to the lower soil moisture content at the grid cell scale used to calculate the soil thermal regime in the model. This limits the modeled heat capacity and thermal conductivity of the soil, ultimately failing to reproduce the zero curtain period. Thus, in order to improve the modeled winter emissions of methane, it is also mandatory to improve the representation of the soil moisture regime in the model.

4.6. Role of non-growing season CH_4 emissions

In this work, we present, to our knowledge, the first simulated CH_4 emissions during the non-growing season with a land surface model at a regional scale. Our results show that changes in the snow layer depth control the temporal variation of the molecular diffusion of CH_4 through the snow. Our sensitivity studies corroborate that setting a thinner layer of snow as a threshold depth to switch to the CH_4 emission process during the cold season only promotes some changes in the partitioning of the methane flux among the four transport pathways. For example, a thinner snow layer promotes an earlier release of CH_4 than was otherwise emitted during late summer with a thicker layer of snow. However, the magnitude of the emissions through the snow is also determined by the amount of CH_4 that is produced, calculated from the decomposed carbon that is driven only by air temperature and precipitation in the Yasso07 module. Changes in the physical properties of the snowpack (i.e. porosity and density) defined in the model have no clear effect on the timing of the emissions through the snow; this may lead to the conclusion that our choice of values for the capacity of snow to transport CH_4 was large enough. The physical restriction of gas transport via diffusive processes mod-

eled by Fick's first law ensures that only physically possible rates of gas transport are being modeled.

In the recent work by Pirk et al. (2016), the authors demonstrated that the fluxes of CH_4 through the snowpack of permafrost Arctic wetlands during wintertime reflected a continuous emission of low amounts of gas still being produced in the soil, rather than solely the release of gas stored in the soil that was produced during the preceding growing season. These observations are in agreement with those from Mast et al. (1998), where the authors reported evidence of microbial activity throughout winter in subalpine soils permitted by the insulating effect of the snow layer. The results of Pirk et al. (2016) showed that there was no apparent sink or source of CH_4 within the snowpack, and their measurements captured a linear concentration gradient through the snowpack (Pirk et al., 2016). This observation validates the application of Fick's first law for diffusion of fluxes through the snow during winter, as applied in our model configuration. However, our formulation does not take into account the "pressure pumping" process reported by Massman et al. (1997) and Bowling and Massman (2011) that is related to the persistent advection of gas enhanced by wind through the snowpack. Based on isotopic analysis of CO_2 through the snowpack of a mountain forest, Bowling and Massman (2011) found that in the presence of wind, the pressure pumping effect contributed up to 11 % of the total emissions during winter.

Our comparison at a grid cell scale to wintertime fluxes measured from eddy covariance at the Chersky floodplain (from January until March 2015 on average 3.8 mg CH_4 m^{-2} d^{-1}) shows that the modeled CH_4 emissions during this season are consistently lower by about one order of magnitude (0.4 mg CH_4 m^{-2} d^{-1}). The measured eddy covariance fluxes are similar to other measurements with other methods from earlier studies. The work by Panikov and Dedysh (2000) showed winter methane emissions measured by chambers of about 5.0 mg CH_4 m^{-2} d^{-1} from boreal peat bogs in western Siberia in mid-February. Pirk et al., (2016) measured CH_4 fluxes above the snowpack of about 2.4 mg CH_4 m^{-2} d^{-1}. In subalpine soils covered with snow, Mast et al. (1998) reported average winter CH_4 emissions of 4.4 mg CH_4 m^{-2} d^{-1} in moist soils calculated from samples collected through the snowpack. However, our modeled winter CH_4 emissions are comparable to those reported by Smagin and Shnyrev (2015) of about 0.6 mg CH_4 m^{-2} d^{-1} measured by chambers during the coldest months of the year (February and March) in environments with different soil wetness in a West-Siberian bog landscape.

Moreover, it is important to note that our results represent average values of a grid cell with a 0.5° x 0.5° horizontal resolution, whereas measurements represent a much smaller spatial

scale. Integrating the latter to the grid cell level must lead to an overestimation of the emission values at the grid cell level.

Other works have reported large CH_4 emissions from dry areas during the non-growing season. Using eddy covariance measurements, Zona et al., (2016) showed large fluxes from dry areas of the Alaskan tundra during the zero curtain period. The findings of Mastepanov et al. (2013) imply that a portion of the active layer still remains free of ice during late autumn, and moisture and temperature changes are limited by the low thermal conductivity and heat capacity of dry soils.

In the model, the consistently lower CH_4 emissions during winter can be linked to multiple factors: a) lower soil temperatures, when compared to the site measurements, due to low soil moisture content, leading to b) low carbon decomposition and, as a result c) poor methane production and larger oxidation within the topsoil, which reduces the amount of methane emissions during the wintertime, and d) the lack of inclusion in the model of the pressure pumping process that accounts for the persistent advection of gas induced by wind through the snowpack. This process might contribute to increasing the modeled emissions of CH_4 during wintertime.

5. Conclusion and outlook

The refined configuration of the JSBACH-methane model presented in this work has the ability to realistically represent year-round CH_4 emissions at a regional scale for a floodplain area located in northeastern Siberia underlain by permafrost. The seasonal transition of four CH_4 transport pathways is mainly controlled by changes in the soil temperature, but only indirectly linked to soil moisture, and is ultimately dependent on the prescribed parameters in the model. The magnitude of the year-round total model CH_4 fluxes is comparable to values measured by chambers and eddy covariance in the same study area, with dominant emissions in the presence of vascular plants. Modeled CH_4 emissions through the snow are still too low when compared to eddy covariance measurements. The reason for this might well lie in the modeled physical state of the soil, which does not match the field conditions, especially in winter. The soil moisture of the ice-free soil pores in the inundated part of the grid cell was set to 95 % saturation, for purposes of justifying inundation in the TOPMODEL approach. Still, the temperature and ice conditions in the soil are not influenced by this change, which in turn leads to a missing link in terms of the distribution of soil water to soil ice or soil moisture. This distribution consequently disagrees with the prescribed constant soil pore moisture. Our model will greatly benefit from further improvements for regional simulations, which will also contribute to advancing the application to a global scale. In summary:

1) Improvements to the dynamics of the snow layer, and the inclusion of other snow properties, e.g. effective thermal conductivity, may benefit the simulation of wintertime CH_4 emissions, and processes, e.g. pressure pumping due to advection of gas enhanced by wind.

2) Improvements to prescribed model parameters such as soil depth until bedrock and initial soil moisture saturation, which are normally obtained from global scale configurations of JSBACH.

3) Improvements to the connection between the TOPMODEL approach and soil conditions such as soil moisture, soil temperature, and ice content, which in turn might lead to improved soil thermal capacity and conductivity of heat.

4) The integrated TOPMODEL scheme in the model allows simulating the inundated fractions in a model grid cell; however, improvements are needed to better represent the temporal transitions and seasonality of the water table levels that will help to better constrain the surface heterogeneity of hydrologic responses to permafrost thaw and the spatial distribution of carbon decomposition.

5) Increasing the horizontal resolution within the regional domain might contribute to improving the steep spatial heterogeneity currently seen between grid cells in the model. This can only be achieved with the availability of highly resolved input boundary parameters and atmospheric forcing data for the Arctic.

6) Currently the model does not explicitly consider other sources and sinks of CH_4 like production from root exudates or within anaerobic microsites confined in oxic soils, as well as anoxic CH_4 oxidation. To advance the explicit parameterization of these processes in land-surface models, one approach would be to include better representations of microbial community composition and dynamics to improve the current and future changes of carbon emissions in northern wetlands influenced by permafrost thaw. However, research on these processes is still ongoing and only robust schemes to represent these processes might be included in future model improvements.

6. Code and data availability

The model code is available upon request to the corresponding author (kcastro@bgc-jena.mpg.de). The eddy covariance datasets will be made available through the European Fluxes Database Cluster. The chamber flux data is available upon request to M. Göckede (mgoeck@bgc-jena.mpg.de).

Biogeosciences Discuss., https://doi.org/10.5194/bg-2017-310
Manuscript under review for journal Biogeosciences
Discussion started: 24 July 2017

7. Appendices

Appendix A: Modifications to JSBACH-methane module

The original JSBACH-methane module presented in Kaiser et al., 2017, underwent several modifications. These are:

i) **Improved description of the plant-mediated transport**: Instead of constraining the methane transport by the root length of gas transporting vascular plants, in this model configuration the gas transported through plants is constrained by the fraction of soil volume that is occupied by plants roots, i.e. the root volume. This modification was done to avoid the possible use of unrealistic values for mean accumulated root lengths that are difficult to assess from field studies. In this new configuration, the actual volume of the soil that is occupied by roots (V_r) is calculated from the available pore space in the soil (i.e. (1- v_p), where v_p is the volumetric soil porosity), and the prescribed principal fraction of the pore-free soil volume filled by roots (R_{fr}), which in turn is constrained by the soil type. In the same way, and as in the original JSBACH-methane model, plant roots are modeled as one cylinder per plant tiller. Thus, the surface area that the plant roots exhibit per layer depth (A_{rl}, in m^2/m^2) within the rooting soil layers, is described as:

$$A_{rl} = \frac{4 \cdot V_r}{d_r} \quad (2)$$

where d_r is the diameter of an individual root, and V_r is defined as:

$$V_r = \left(1 - v_p\right) \cdot R_{fr} \cdot h \cdot \frac{LAI}{\max\left(LAI\right)} \quad (3)$$

where h is the soil layer height, and LAI is the varying leaf area index; thus, the last term of Eq. 3 determines the growing state of the plants. The amount of methane that is emitted through plants ($n_{plant}^{CH_4}$) remains as in Eq. 7 of Kaiser et al. (2017):

$$n_{plant}^{CH_4} = D_r^{CH_4} \cdot \left(c^{CH_4} - c_{air}^{CH_4}\right) \cdot \frac{1}{h_{exo}} \cdot \mathrm{d}t \cdot A_{rl} \cdot f_r \quad (4)$$

where $D_r^{CH_4}$ is the diffusion coefficient of the root exodermis for methane, which is defined as 80 % of the diffusion coefficient for CH_4 in water, D_w (i.e. $D_r = 0.8\ D_w$, where 0.8 is meant as a factor of resistance r of the root exodermis to gas transfer), c^{CH4} is the concentration of methane in the soil, $c_{air}^{CH_4}$ is the atmospheric methane concentration, h_{exo} is the thickness of the exodermis, dt is the time step, and f_r is the fraction of roots able to transport gases, which is set to ~83 % based on the same criteria of *Carex aquatilis* dominance over the dominance of total vascular plants in a square meter of wet soils, i. e. $f_r = \frac{dominance\ C.\ aquatilis}{dominance\ vasc.\ plants} = \frac{25}{30}$ (Kutzbach et al., 2004). Positive values of $n_{plant}^{CH_4}$ represent emissions of gas from the soil into

the atmosphere. The formulation for oxygen uptake through plants is the same as in Eq. 6 of Kaiser et al., 2017, but with opposite sign convention (i.e. here, negative values mean uptake of gas from the atmosphere into the soil).

The transport of gas through plants is a two-way simultaneous pathway, with a flux of oxygen and methane between the atmosphere and pore spaces in the soil layers. Transport of methane through plants will take place as long as there is sufficient gas in the soil pockets to diffuse through the plant exodermis. The gradient of the gas concentrations is evaluated at every time step until it equals zero. At this point, the concentration of gas in the soil (i.e. in soil air and soil moisture combined) is equal to the so-called equilibrium concentration. That is the combined concentration in the soil air and in the soil moisture that would be in equilibrium with the concentration in atmospheric air according to Henry's Law. Thus, the magnitude of the two-way plant-mediated transport of oxygen and methane is explicitly restricted by the equilibrium concentration of these gases in the soil pores.

In this model configuration, we consider the cotton grass *Eriophorum angustifolium* as the plant species dominating plant-mediated transport in the natural environment conditions of the Chersky floodplain (Kwon et al., 2016). The prescribed constant d_r value is equal to 2 mm, considering a predominance of fine roots, and R_{fr} = 40 % (i.e. from the total available pore-free soil volume, 40 % will be occupied by roots). The model's response to changes in prescribed values for d_r and f_r is evaluated as part of sensitivity tests described in section 2.2.2.

ii) **Gas transport through the snow**: In this model version, we include the transport of gas through snow during the cold season. Similar to the root exodermis in the plant-mediated transport, the snow is a barrier where gases can move through only by molecular diffusion. Thus, the diffusion of a gas through snow can be related to Fick's first law. The effective diffusion coefficient of a gas species x in snow D_{eff}^{x} (i.e. D_{eff}^{CH4} for methane and D_{eff}^{O2} for oxygen) is related to the dimensionless snow porosity ϕ, the dimensionless tortuosity factor τ, and the diffusion coefficient of the gas in air D_{air}^{x}:

$$D_{eff}^{x} = D_{air}^{x}\, \phi\, \tau \left(\frac{P_0}{P}\right)\left(\frac{T}{T_0}\right)^{1.81} \quad (5)$$

where $D_{air}^{CH_4}$ = 1.95×10^{-5} m^2 s^{-1} and $D_{air}^{O_2}$ = 1.82×10^{-5} m^2 s^{-1}, both at reference temperature T_0 (273.15 K) and pressure P_0 (1013.3 hPa). The term D_{air}^{x}, should be corrected by the pressure P and the temperature T of the snowpack, as shown in the fourth and fifth terms of Eq. 5 (Mast et al., 1998; Pirk et al., 2016). However, because the model does not explicitly simulate the snowpack thermophysical properties, D_{air}^{x} is not corrected by the P and T values of the

snowpack but by those values in the first soil layer. The snow porosity ϕ is the fraction of the snowpack that is occupied by air and is determined by the ratio of the densities of snow (ρ_{snow} = 330 kg/m^3) to ice (ρ_{ice} = 910 kg/m^3) as: $\phi = 1 - \frac{\rho_{snow}}{\rho_{ice}}$ (Wickland et al., 1999). τ is defined as the ratio of the path length in the porous medium over the direct path length (Domine et al., 2008), and is calculated as a function of ϕ (Pirk et al., 2016):

$$\tau = \frac{1-(1-\phi)^{2/3}}{\phi} \quad (6)$$

Thus there will be more tortuosity for the gas molecules as more pore space is available. In reality, D^x_{eff} varies through the snow pack in relation to the depth of the snow layer. Chemically reactive gases may undergo adsorption and desorption in the snow grain surface, especially if the snow layer is deep and compacted, allowing gas retention for a period of time in the interstitial space and potential chemical transformation (Domine et al., 2008), thus also affecting the values of D^x_{eff}. Here, we simplified the scheme by considering both CH_4 and O_2 as inert gases during their molecular diffusion through the layer of snow with constant ϕ and consequently constant D^x_{eff}. For methane, the amount of transferred gas through snow (n^{CH4}_{snow} in mol m^{-2} h^{-1}) is thus represented as:

$$n^{CH_4}_{snow} = D^{CH_4}_{eff} \cdot \left(c^{CH_4} - c^{CH_4}_{eq}\right) \cdot \frac{1}{dz} \cdot dt \quad (7)$$

where c^{CH4} and $c^{CH_4}_{eq}$ are the methane concentration in the top soil layer and the equilibrium concentration as defined above, and dz is the snow depth. Positive values are emissions of CH_4 into the atmosphere. The same formulation applies for oxygen by replacing the second term with $\left(c^{O_2}_{eq} - c^{O_2}\right)$ due to the sign convention of the gas emissions, leading to positive values, in this case, for oxygen uptake from the atmosphere.

In the model, gases can be transported through a snow layer of defined thickness via snow diffusion (snow threshold depth, h_{snow}). Gas transport through the snow will take place only if $h_{snow} \geq 5$ cm, while under these conditions, emission, or uptake by other processes is prohibited, following the original JSBACH-methane configuration of Kaiser et al. (2017). Conversely, in summer, transport via diffusion through snow is prohibited when $h_{snow} < 5$ cm, but transport via ebullition, ordinary molecular diffusion, and plant-mediated transport may take place. As done in the plant-mediated transport, a similar explicit restriction of gas transport is also used here to prohibit the diffusion once the concentration gradient between the soil pore spaces and the atmosphere is zero (i.e. equilibrium conditions). Both h_{snow} and ϕ are parameters in the model used to restrict the transport of gas via diffusion through snow during the

cold season, and assessments of the model sensitivity to changes in the values of these parameters were done in this work.

iii) **Order of emission processes**: In the JSBACH-methane module, the transport pathways occur sequentially, i.e. one after the other, taking care of mass conservation in each model iteration. In the original model version, the order of the transport pathways was: ebullition, molecular diffusion and plant-mediated transport. This order was set by taking the relative speed of each process into consideration. In contrast, in this model configuration, the order of processes is: plant-mediated transport, molecular diffusion, and ebullition. This new order of processes was chosen by taking their expected share in the total emissions into consideration and was done mainly to improve the small contribution that plant-mediated transport had in the original JSBACH-methane module. The aerenchyma structures of plants in wetlands are an efficient exit route for CH_4 to the atmosphere, bypassing zones of aerobic oxidation. Previous studies have demonstrated that in the presence of vascular plants in Arctic permafrost tundra ecosystems, plant-mediated transport is the dominating methane transport pathway over ebullition and diffusion (Knoblauch et al., 2016), and this transport pathway can contribute from 30 to 100 % to the total CH_4 flux (Bridgham et al., 2013).

Molecular diffusion is in the second position of the methane transport pathways. Despite the fact that in nature the amount of methane emitted through this pathway is lower than that emitted via ebullition and plant transport, it takes place throughout the year and is not limited by other factors such as plant root tissues. Finally, ebullitive methane fluxes were considered in the last position of the sequence of CH_4 transport processes in the model. The amount of methane emitted via ebullition can be significant and can exceed by orders of magnitude the amount of gas emitted via plants and by molecular diffusion (e.g. Tokida et al., 2007). However, ebullition is a rapid process that is highly variable temporally and spatially. Observations have shown that CH_4 emitted through ebullition occurs sporadically and mainly in undisturbed natural water bodies, such as lakes and ponds, where gas bubbles formed during active methanogenesis ascend rapidly through the water and into the atmosphere, circumventing aerobic soil layers (Klapstein et al., 2014; Knoblauch et al., 2016). Thus, by leaving this process in the last position we ensured that the small amounts of CH_4 transported by molecular diffusion can work properly. In contrast, gas transport via diffusion through the snow will take place under conditions of considerably high snow depth aboveground as discussed above in point ii) of this section, and thus does not compete with the other transport processes.

8. Special issue statement

This manuscript is a contribution to the special issue dedicated to the project: "Changing Permafrost in the Arctic and its Global Effects in the 21st Century (PAGE21)".

9. Acknowledgements

This work was supported through funding by the European Commission (PAGE21 project, FP7-ENV-2011, Grant Agreement No. 282700, and PerCCOM project, FP7-PEOPLE-2012-CIG, Grant Agreement No. PCIG12-GA-201-333796), the German Ministry of Education and Research (CarboPerm-Project, BMBF Grant No. 03G0836G), and the AXA Research Fund (PDOC_2012_W2 campaign, ARF fellowship M. Göckede). KCM wishes to thank Andrew Durso for the English proofread of this manuscript.

10. References

Beer, C.: Soil science: the Arctic carbon count, Nature geoscience, 1, 569-570, 2008, 10.1038/ngeo292.

Beven, K. J. and Kirkby, M. J.: A physically based, variable contributing area model of basin hydrology, Hydrological Sciences Bulletin, 24, 43-69, 1979, 10.1080/02626667909491834.

Blanc-Betes, E., Welker, J. M., Sturchio, N. C., Chanton, J. P., and Gonzalez-Meler, M. A.: Winter precipitation and snow accumulation drive the methane sink or source strength of Arctic tussock tundra, Global Change Biology, 22, 2818-2833, 2016, 10.1111/gcb.13242.

Bohn, T. J., Melton, J. R., Ito, A., Kleinen, T., Spahni, R., Stocker, B. D., Zhang, B., Zhu, X., Shroeder, R., Glagolev, M. V., Maksyutov, S., Brovkin, V., Chen, G., Denisov, S. N., Eliseev, A. V., Gallego-Sala, A., McDonald, K. C., Rawlins, M. A., Riley, W. J., Subin, Z. M., Tian, H., Zhuang, Q., and Kaplan, J. O.: WETCHIMP-WSL: intercomparison of wetland methane emissions models over West Siberia, Biogeosciences, 12, 3321-3349, 2015, 10.5194/bg-12-3321-2015.

Bowling, D. R. and Massman, W. J.: Persistent wind-induced enhancement of diffusive CO_2 transport in a mountain forest snowpack, Journal of Geophysical Research, 116, G04006, 2011, 10.1029/2011JG001722.

Braakhekke, M. C., Beer, C., Hoosbeek, M. R., Reichstein, M., Kruijt, B., Schrumpf, M., and Kabat, P.: SOMPROF: A vertically explicit soil organic matter model, Ecological Modelling, 222, 1712-1730, 2011, 10.1016/j.ecolmodel.2011.02.015.

Braakhekke, M. C., Beer, C., Schrumpf, M., Ekici, A., Ahrens, B., Hoosbeek, M. R., Kruijt, B., Kabat, P., and Reichstein, M.: The use of radiocarbon to constrain current and future soil organic matter turnover and transport in a temperate forest, Journal of Geophysical Research: Biogeosciences, 119, 372-391, 2014, 10.1002/2013JG002420.

Braakhekke, M. C., Wutzler, T., Beer, C., Kattge, J., Schrumpf, M., Ahrens, B., Schöning, I., Hoosbeek, M. R., Kruijt, B., Kabat, P., and Reichstein, M.: Modeling the vertical soil organic

matter profile using Bayesian parameter estimation, Biogeosciences, 10, 399-420, 2013, 10.5194/bg-10-399-2013.

Bridgham, S. D., Cadillo-Quiroz, H., Keller, J. K., and Zhuang, Q.: Methane emissions from wetlands: biogeochemical, microbial, and modeling perspectives from local to global scales, Global Change Biology, 19, 1325-1346, 2013, 10.1111/gcb.12131.

Brovkin, V., Boysen, L., Raddatz, T., Gayler, V., Loew, A., and Claussen, M.: Evaluation of vegetation cover and land-surface albedo in MPI-ESM CMIP5 simulations, Journal of Advances in Modeling Earth Systems, 5, 48-57, 2013, 10.1029/2012MS000169.

Chang, R. Y. W., Miller, C. E., Dinardo, S. J., Karion, A., Sweeney, C., Daube, B. C., Henderson, J. M., Mountain, M. E., Eluszkiewicz, J., Miller, J. B., Bruhwiler, L. M. P., and Wofsy, S. C.: Methane emissions from Alaska in 2012 from CARVE airborne observations, Proceedings of the National Academy of Sciences, 111, 16694-16699, 2014, 10.1073/pnas.1412953111.

Chen, X., Bohn, T. J., and Lettenmaier, D. P.: Model estimates of climate controls on pan-Arctic wetland methane emissions, Biogeosciences, 12, 6259-6277, 2015, 10.5194/bg-12-6259-2015.

Christensen, T. R., Johansson, T., Akerman, H. J., and Mastepanov, M.: Thawing sub-arctic permafrost: effects on vegetation and methane emissions, Geophysical Research Letters, 31, L04501, 2004, 10.1029/2003GL018680.

Conrad, R.: Contribution of hydrogen to methane production and control of hydrogen concentrations in methanogenic soils and sediments, FEMS Microbiology Ecology, 28, 193-202, 1999, 10.1111/j.1574-6941.1999.tb00575.x.

Domine, F., Albert, M., Huthwelker, T., Jacobi, H.-W., Kokhanovsky, A. A., Lehning, M., Picard, G., and Simpson, W. R.: Snow physics as relevant to snow photochemistry, Atmospheric Chemistry and Physics, 8, 171-208, 2008, 10.5194/acp-8-171-2008.

Domine, F., Barrere, M., Sarrazin, D., Morin, S., and Arnaud, L.: Automatic monitoring of the effective thermal conductivity of snow in a low-Arctic shrub tundra, The Cryosphere, 9, 1265-1276, 2015, 10.5194/tc-9-1265-2015.

Dutta, K., Schuur, E. A., Neff, J. C., and Zimov, N.: Potential carbon release from permafrost soils of Northeastern Siberia, Global Change Biology, 12, 2336-2351, 2006, 10.1111/j.1365-2486.2006.01259.x.

Ekici, A., Beer, C., Hagemann, S., Boike, J., Langer, M., and Hauck, C.: Simulating high-latitude permafrost regions by the JSBACH terrestrial ecosystem model, Geoscientific Model Development, 7, 631-647, 2014, 10.5194/gmd-7-631-2014.

Friborg, T., Christensen, T. R., and Sogaard, H.: Rapid response of greenhouse gas emission to early spring thaw in a subarctic mire as shown by micrometeorological techniques, Geophysical Research Letters, 24, 3061-3064, 1997, 10.1029/97GL03024.

Göckede, M., Kittler, F., Kwon, M. J., Burjack, I., Heimann, M., Kolle, O., Zimov, N., and Zimov, S.: Shifts in permafrost ecosystem structure following a decade-long drainage

increase energy transfer to the atmosphere, but reduce thaw depth, The Cryosphere Discussions, doi: 10.5194/tc-2016-212, 2017. 2017, 10.5194/tc-2016-212.

Goll, D. S., Brovkin, V., Liski, J., Raddatz, T., Thum, T., and Todd-Brown, K. E. O.: Strong dependence of CO_2 emissions from anthropogenic land cover change on initial land cover and soil carbon parameterization, Global Biogeochemical Cycles, 29, 1511-1523, 2015, 10.1002/2014GB004988.

Grant, R. F.: Simulation of methanogenesis in the mathematical model Ecosys, Soil Biology and Biochemistry, 30, 883-896, 1998, 10.1016/S0038-0717(97)00218-6.

Hagemann, S. and Stacke, T.: Impact of the soil hydrology scheme on simulated soil moisture memory, Climate Dynamics, 44, 1731-1750, 2015, 10.1007/s00382-014-2221-6.

Hugelius, G., Strauss, J., Zubrzyicki, S., Harden, J. W., Schuur, E. A., Ping, C.-L., Schirrmeister, L., Grosse, G., Michaelson, G. J., Koven, C. D., O'Donell, J. A., Elberling, B., Mishra, U., Camill, P., Yu, Z., Palmtag, J., and Kuhry, P.: Estimated stocks of circumpolar permafrost carbon with quantified uncertainty ranges and identified data gaps, Biogeosciences, 11, 6573-6593, 2014, 10.5194/bg-11-6573-2014.

Jammet, M., Crill, P., Dengel, S., and Friborg, T.: Large methane emissions from a subarctic lake during spring thaw: mechanisms and landscape significance, Journal of Geophysical Research: Biogeosciences, 120, 2289-2305, 2015, 10.1002/2015JG003137.

Kaiser, S., Göckede, M., Castro-Morales, K., Knoblauch, C., Ekici, A., Kleinen, T., Zubrzycki, S., Sachs, T., Wille, C., and Beer, C.: Process-based modelling of the methane balance in periglacial landscapes (JSBACH-methane), Geoscientific Model Development, 10, 333-358, 2017, 10.5194/gmd-10-333-2017.

Kattsov, V. M. and Walsh, J. E.: Twentieth-century trends of Arctic precipitation from observational data and climate model simulation, Journal of Climate, 13, 1362-1370, 2000, 10.1175/1520-0442(2000)013<1362:TCTOAP>2.0.CO;2.

Kim, Y., Ueyama, M., Nakagawa, F., Tsunogai, U., Harazono, Y., and Tanaka, N.: Assessment of winter fluxes of CO_2 and CH_4 in boreal forest soils of central Alaska estimated by the profile method and the chamber method: a diagnosis of methane emission and implications for the regional carbon budget, Tellus, 59B, 223-233, 2007, 10.1111/j.1600-0889.2006.00233.x.

Kirkby, M. J.: Hydrograph modelling strategies. In: Process in Physical and Human Geography, Peel, R., Chisholm, M., and Hagget, P. (Eds.), Heinemann, London, 1975.

Kittler, F., Burjack, I., Corradi, C. A. R., Heimann, M., Kolle, O., Merbold, L., Zimov, N., Zimov, S., and Göckede, M.: Impacts of a decadal drainage disturbance on surface-atmosphere fluxes of carbon dioxide in a permafrost ecosystem, Biogeosciences, 13, 5315-5332, 2016, 10.5194/bg-13-5315-2016.

Klapstein, S. J., Turetsky, M. R., McGuire, D., Harden, J. W., Czimiczik, C. I., Xu, X., Chanton, J. P., and Waddington, J. M.: Controls on methane released through ebullition in peatlands affected by permafrost degradation, Journal of Geophysical Research: Biogeosciences, 119, 418-431, 2014, 10.1002/2013JG002441.

Kleinen, T., Brovkin, V., and Schuldt, R. J.: A dynamic model of wetland extent and peat accumulation: results for the Holocene, Biogeosciences, 9, 235-248, 2012, 10.5194/bg-9-235-2012.

Knoblauch, C., Spott, O., Evgrafova, S., Kutzbach, L., and Pfeiffer, E.-M.: Regulation of methane production, oxidation, and emission by vascular plants and bryophytes in ponds of the northeast Siberian polygonal tundra, Journal of Geophysical Research: Biogeosciences, 120, 2525-2541, 2016, 10.1002/2015JG003053.

Knorr, W.: Annual and interannual CO_2 exchanges of the terrestrial biosphere: process-based simulations and uncertainties, Global Ecology and Biogeography, 9, 225-252, 2000, 10.1046/j.1365-2699.2000.00159.x.

Koven, C. D., Lawrence, D. M., and Riley, W. J.: Permafrost carbon-climate feedback is sensitive to deep soil carbon decomposability but not deep soil nitrogen dynamics, Proceedings of the National Academy of Sciences, 112, 3752-3757, 2015, 10.1073/pnas.1415123112.

Kutzbach, L., Wagner, D., and Pfeiffer, E.-M.: Effect of microrelief and vegetation on methane emission from wet polygonal tundra, Lena Delta, Northern Siberia, Biogeochemistry, 69, 341-362, 2004, 10.1023/B:BIOG.0000031053.81520.db.

Kwon, M. J., Beulig, F., Ilie, I., Wildner, M., Küsel, K., Merbold, L., Mahecha, M. D., Zimov, N., Zimov, S. A., Heimann, M., Schuur, E. A., Kostka, J. E., Kolle, O., Hilke, I., and Göckede, M.: Plants, microorganisms, and soil temperatures contribute to a decrease in methane fluxes on a drained Arctic floodplain, Global Change Biology, 23, 2396-2412, 2016, 10.1111/gcb.13558.

Lawrence, D. M., Koven, C. D., Swenson, S. C., Riley, W. J., and Slater, G.: Permafrost thaw and resulting soil moisture changes regulate projected high-latitude CO_2 and CH_4 emissions, Environmental Research Letters, 10, 094011, 2015, 10.1088/1748-9326/10/9/094011.

Liljedahl, A. K., Boike, J., Daanen, R. P., Fedorov, A. N., Frost, G. V., Grosse, G., Hinzman, L. D., Lijma, Y., Jorgenson, J. C., Matveyeva, N., Necsoiu, M., Raynolds, M. K., Romanovsky, V. E., Schulla, J., Tape, K. D., Walker, D. A., Wilson, C. J., Yabuki, H., and Zona, D.: Pan-Arctic ice-wedge degradation in warming permafrost and its influence on tundra hydrology, Nature geoscience, 9, 2016, 10.1038/NGEO2674.

Marthews, T. R., Dadson, S. J., Lehner, B., Abele, S., and Gedney, N.: High-resolution global topographic index values for use in large-scale hydrological modelling, Hydrology and Earth System Sciences, 19, 91-104, 2015, 10.5194/hess-19-91-2015.

Massman, W. J., Sommerfeld, R. A., Mosier, A. R., Zeller, K. F., Hehn, T. J., and Rochelle, S. G.: A model investigation of turbulence-driven pressure-pumping effects on the rate of diffusion of CO_2, N_2O, and CH_4 through layered snowpacks, Journal of Geophyscial Research, 102, 18851-18863, 1997, 10.1029/97JD00844.

Mast, M. A., Wickland, K. P., Striegl, R. T., and Clow, D. W.: Winter fluxes of CO_2 and CH4 from subalpine soils in Rocky Mountain National Park, Colorado, Global Biogeochemical Cycles, 12, 607-620, 1998, 10.1029/98GB02313.

Mastepanov, M., Sigsgaar, C., Tagesson, T., Ström, L., Tamstorf, M. P., and Christensen, T. R.: Revisiting factors controlling methane emissions from high-Arctic tundra, Biogeosciences, 10, 5139-5158, 2013, 10.5194/bg-10-5139-2013.

Mastepanov, M., Sigsgaard, C., Dlugokencky, E. J., Houweling, S., Ström, L., Tamstorf, M. P., and Christensen, T. R.: Large tundra methane burst during onset of freezing, Nature, 456, 628-631, 2008, 10.1038/nature07464.

McCalley, C. K., Woodcroft, B. J., Hodgkins, S. B., Wehr, R. A., Kim, E.-H., Mondav, R., Crill, P. M., Chanton, J. P., Rich, V. I., Tyson, G. W., and Saleska, S. R.: Methane dynamics regulated by microbial community response to permafrost thaw, Nature, 514, 478-481, 2014, 10.1038/nature13798.

Melton, J. R., Wania, R., Hodson, E., Poulter, B., Ringeval, B., Spahni, r., Bohn, T., Avis, C. A., Beerling, D. J., Chen, G., Eliseev, A. V., Denisov, S. N., Hopcroft, P. O., Lettenmaier, D. P., Riley, W. J., Singarayer, J. S., Subin, Z. M., Tian, H., Zurcher, S., Brovkin, V., van Bodegom, P. M., Kleinen, T., Yu, Z., and Kaplan, J. O.: Present state of global wetland extent and wetland methane modelling: conclusion from a model intercomparison project (WETCHIMP), Biogeosciences, 10, 753-788, 2013, 10.5194/bg-10-753-2013.

Merbold, L., Kutsch, W. L., Corradi, C., Kolle, O., Rebmann, C., Stoy, P. C., Zimov, S. A., and Schulze, E.-D.: Artificial drainage and associated carbon fluxes (CO_2/CH_4) in a tundra ecosystem, Global Change Biology, 15, 2599-2614, 2009, 10.1111/j.1365-2486.2009.01962.x.

Mi, Y., van Huissteden, J., Parmentier, F.-J. W., Gallagher, A., Budishchev, A., Berridge, C. T., and Dolman, A. J.: Improving a plot-scale methane emission model and its performance at a northeastern Siberian tundra site, Biogeosciences, 11, 3985-3999, 2014, 10.5194/bg-11-3985.

Panikov, N. S. and Dedysh, S. N.: Cold season CH_4 and CO_2 emission from boreal peat bogs (West Siberia): winter fluxes and thaw activation dynamics, Global Biogeochemical Cycles, 14, 1071-1080, 2000, 10.1029/1999BG900097.

Pirk, N., Tamstorf, M. P., Lund, M., Mastepanov, M., Pedersen, S. H., Mylius, M. R., Parmentier, F.-J. W., Christiansen, H. H., and Christensen, T. R.: Snowpack luxes of methane and carbon dioxide from high Arctic tundra, Journal of Geophysical Research: Biogeosciences, 121, 2016, 10.1002/2016JG003486.

Preuss, I., Knoblauch, C., Gebert, J., and Pfeiffer, E.-M.: Improved quantification of microbial CH_4 oxidation efficiency in Arctic wetland soils using carbon isotope fractionation, Biogeosciences, 10, 2539-2552, 2013, 10.5194/bg-10-2539-2013.

Prigent, C., Papa, F., Aires, F., Rossow, W., and Matthews, E.: Global inundation dynamics inferred from multiple satellite observations, 1993-2000, Journal of Geophysical Research, 112, 2007, 10.1029/2006JD007847.

Raddatz, T., Reick, C., Knorr, W., Kattge, J., Roeckner, E., Schnur, R., Schnitzler, K.-G., Wetzel, P., and Jungclaus, J.: Will the tropical land biosphere dominate the climate-carbon cycle feedback during the twenty-first century?, Climate Dynamics, 29, 565-574, 2007, 10.1007/s00382-007-0247-8.

Reick, C., Raddatz, T., Brovkin, V., and Gayler, V.: Representation of natural and anthropogenic land cover change in MPI-ESM, Journal of Advances in Modeling Earth Systems, 5, 459-482, 2013, 10.1002/jame.20022.

Reschke, J., Bartsch, A., Schlaffer, S., and Schepaschenko, D.: Capability of C-Band SAR for Operational Wetland Monitoring at High Latitudes, Remote Sensing, 4, 2923-2943, 2012, 10.3390/rs4102923.

Riley, W. J., Subin, Z. M., Lawrence, D. M., Swenson, S. C., Torn, M. S., Meng, L., Mahowald, N. M., and Hess, P.: Barriers to predicting changes in global terrestrial methane fluxes: analyses using CLM4Me, a methane biogeochemistry model integrated in CESM, Biogeosciences, 8, 1925-1953, 2011, 10.5194/bg-8-1925-2011.

Ringeval, B., Friedlingstein, P., Koven, C., Ciais, P., de Noblet-Ducoudré, N., Decharme, B., and Cadule, P.: Climate-CH_4 feedback from wetlands and its interaction with the climate-CO_2 feedback, Biogeosciences, 8, 2137-2157, 2011, 10.5194/bg-8-2137-2011.

Rinne, J., Riutta, T., Pihlatie, M., Aurela, M., Haapanala, S., Tuovinen, J.-P., Tuittila, E.-S., and Vesala, T.: Annual cycle of methane emission from a boreal fen measured by eddy covariance technique, Tellus, 59B, 449-457, 2007, 10.1111/j.1600-0889.2007.00261.x.

Sachs, T., Giebels, M., Boike, J., and Kutzbach, L.: Environmental controls on CH_4 emission from polygonal tundra on the microsite scale in the Lena river delta, Siberia, Global Change Biology, 16, 3096-3110, 2010, 10.1111/j.1365-2486.2010.02232.x.

Saunois, M. and al., e.: The global methane budget 2000-2012, Earth System Science Data, 8, 697-751, 2016, 10.5194/essd-8-697-2016.

Schuldt, R. J., Brovkin, V., Kleinen, T., and Winderlich, J.: Modelling Holocene carbon accumulation and methane emissions of boreal wetlands - an Earth system model approach, Biogeosciences, 10, 1659-1674, 2013, 10.5194/bg-10-1659-2013.

Schuur, E. A., Bockheim, J., Canadell, J. G., Euskirchen, E., Field, C. B., Goryachkin, V., Hagemann, S., Kuhry, P., Lafleur, P. M., Lee, H., Mazhitova, G., Nelson, F. E., Rinke, A., Romanovsky, V. E., Shiklomanov, N., Tarnocai, C., Venevsky, S., Vogel, J. G., and Zimov, S.: Vulnerability of permafrost carbon to climate change: implications for the global carbon cycle, BioScience, 58, 701-714, 2008, 10.1641/B580807.

Schuur, E. A., McGuire, D., Schädel, C., Grosse, G., Harden, J. W., Hayes, D. J., Hugelius, G., Koven, C. D., Kuhry, P., Lawrence, D. M., Natali, S. M., Olefeldt, D., Romanovsky, V. E., Schaefer, K., Turetsky, M. R., Treat, C. C., and Vonk, J. E.: Climate change and the permafrost carbon feedback, Nature, 520, 171-179, 2015, 10.1038/nature14338.

Serreze, M. C., Walsh, J. E., Chapin III, F. S., Osterkamp, T. E., Dyurgerov, M., Romanovsky, V., Oechel, W. C., Morison, J., Zhang, T., and Barry, R. G.: Observational evidence of recent change in the Northern high-latitude environment, Climatic Change, 46, 159-207, 2000, 10.1023/A:1005504031923.

Sivapalan, M., Beven, K., and Wood, E. F.: On hydrologic similarity 2. A scaled model of storm runoff production, Water Resources Research, 23, 2266-2278, 1987, 10.1029/WR023i012p02266.

Smagin, A. V. and Shnyrev, N. A.: Methane fluxes during the cold season: distribution and mass transfer in the snow cover of bogs, Eurasian Soil Science, 48, 823-830, 2015, 10.1134/S1064229315080086.

Song, C., Xu, X., Sun, X., Tian, H., Sun, L., Miao, Y., Wang, X., and Guo, Y.: Large methane emission upon spring thaw from natural wetlands in the northern permafrost region, Environmental Research Letters, 7, 2012, 10.1088/1748-9326/7/3/034009.

Stocker, B. D., Spahni, R., and Joos, F.: DYPTOP: a cost-efficient TOPMODEL implementation to simulate sub-grid spatio-temporal dynamics of global wetlands and peatlands, Geoscientific Model Development, 7, 3089-3110, 2014, 10.5194/gmd-7-3089-2014.

Ström, L., Tagesson, T., Mastepanov, m., and Christensen, T. R.: Presence of *Eriophorum scheuchyeri* enhances substrate availability and methane emission in an Arctic wetland, Soil Biology and Biogeochemistry, 45, 61-70, 2012, 10.10/j.soilbio.2011.09.005.

Sturtevant, C. S., Oechel, W. C., Kim, Y., and Emerson, C. E.: Soil moisture control over autumn season methane flux, Arctic Coastal Plain of Alaska, Biogeosciences, 9, 1423-1440, 2012, 10.5194/bg-9-1423-2012.

Tagesson, T., Mastepanov, M., Mölder, M., Tamstorf, M. P., Eklundh, L., Smith, B., Sigsgaard, C., Lund, M., Ekber, A., Falk, J. M., Friborg, T., Christensen, T. R., and Ström, L.: Modelling of growing season methane fluxes in a high-Arctic wet tundra ecosystem 1997-2010 using in situ and high-resolution satellite data, Tellus B, 65, 19722, 2013, 10.3402/tellusb.v65i0.19722.

Tarnocai, C., Canadell, J. G., Schuur, E. A., Kuhry, P., Mazhitova, G., and Zimov, S.: Soil organic carbon pools in the northern circumpolar permafrost region, Global Biogeochemical Cycles, 23, GB2023, 2009, 10.1029/2008GB003327.

Thum, T., Räisänen, P., Sevanto, S., Tuomi, M., Reick, C., Vesala, T., Raddatz, T., Aalto, T., Järvinen, H., Altimir, N., Pilegaard, K., Nagy, Z., Rambal, S., and Liski, J.: Soil carbon model alternatives for ECHAM5/JSBACH climate model: evaluation and impacts on global carbon cycle estimates, Journal of Geophysical Research, 116, G02028, 2011, 10.1029/2010JG001612.

Tokida, T., Mizoguchi, M., Miyazaki, T., Kagemoto, A., Nagata, O., and Hatano, R.: Episodic release of methane bubbles from peatland during spring thaw, Chemosphere, 70, 165-171, 2007, 10.1016/j.chemosphere.2007.06.042.

Tuomi, M., Laiho, R., Repo, A., and Liski, J.: Wood decomposition model for boreal forests, Ecological Modelling, 222, 709-718, 2011, 10.1016/j.ecolmodel.2010.10.025.

Tuomi, M., Thum, T., Järvinen, H., Fronzek, S., Berg, B., Harmon, M., Trofymow, J. A., Sevanto, S., and Liski, J.: Leaf litter decomposition - estimates of global variability based on Yasso07 model, Ecological Modelling, 220, 3362-3371, 2009, 10.1016/j.ecolmodel.2009.05.016.

Viovy, N. and Ciais, P.: CRUNCEP data set for 1901-2015, Version 7.0, https://esgf.extra.cea.fr/thredds/catalog/store/p529viov/cruncep/V7_1901_2015/catalog.html, 2016.

Wahlen, S. C. and Reeburgh, W. S.: Interannual variations in tundra methane emission: a 4-year time series at fixed sites, Global Biogeochemical Cycles, 6, 139-159, 1992, 10.1029/92GB00430.

Wahlen, S. C. and Reeburgh, W. S.: Methane oxidation, production, and emission at contrasting sites in a boreal bog, Geomicrobiology Journal, 17, 237-251, 2000, 10.1080/01490450050121198.

Walter, B. P. and Heimann, M.: A process-based, climate-sensitive model to derive methane emissions from natural wetlands: application to five wetland sites, sensitivity to model parameters, and climate, Global Biogeochemical Cycles, 14, 745-765, 2000, 10.1029/1999GB001204.

Wania, R., Ross, I., and Prentice, I. C.: Implementation and evaluation of a new methane model within a dynamic global vegetation model: LPJ-WHyMe v1.3.1, Geoscientific Model Development, 3, 565-584, 2010, 10.5194/gmd-3-565-2010.

Wickland, K. P., Striegl, R. G., Schmidt, S. K., and Mast, M. A.: Methane flux in subalpine wetland and unsaturated soils in the southern Rocky Mountains, Global Biogeochemical Cycles, 13, 101-113, 1999, 10.1029/1998GB900003.

Wille, C., Kutzbach, L., Sachs, T., Wagner, D., and Pfeiffer, E.-M.: Methane emission from Siberian arctic polygonal tundra: eddy covariance measurements and modeling, Global Change Biology, 14, 1395-1408, 2008, j.1365-2486.2008.01586.x.

Xu, X., Elias, D. A., Graham, D. E., Phelps, T. J., Carroll, S. L., Wullschleger, S. D., and Thornton, P. E.: A microbial functional group-based module for simulating methane production and consumption: application to an incubated permafrost soil, Journal of Geophysical Research: Biogeosciences, 120, 1315-1333, 2015, 10.1002/2015JG002935.

Xu, X., Riley, W. J., Koven, C. D., Billesbach, D. P., Chang, R. Y.-W., Commane, R., Euskirchen, E. S., Hartery, S., Harazono, Y., Iwata, H., McDonald, K. C., Miller, C. E., Oechel, W. C., Poulter, B., Raz-Yaseef, N., Sweeney, C., Torn, M., Wofsy, S. C., Zhang, Z., and Zona, D.: A multi-scale comparison of modeled and observed seasonal methane emissions in northern wetlands, Biogeosciences, 13, 5043-5056, 2016, 10.5194/bg-13-5043-2016.

Zhu, Q., Liu, J., Peng, C., Chen, H., Fang, X., Jiang, H., Yang, G., Zhu, D., Wang, W., and Zhou, X.: Modelling methane emissions from natural wetlands by development and application of the TRIPLEX-GHG model, Geoscientific Model Development, 7, 981-999, 2014, 10.5194/gmd-7-981-2014.

Zona, D., Gioli, B., Commane, R., Lindaas, J., Wofsy, S. C., Miller, C. E., Dinardo, S. J., Dengel, S., Sweeney, C., Karion, A., Chang, R. Y.-W., Henderson, J. M., Murphy, P. C., Goodrich, J. P., Moreaux, V., Liljedahl, A., Watts, J. D., Kimball, J. S., Lipson, D. A., and Oechel, W. C.: Cold season emissions dominate the Arctic tundra methane budget, Proceedings of the National Academy of Sciences, 113, 40-45, 2016, 10.1073/pnas.1516017113.

Biogeosciences Discuss., https://doi.org/10.5194/bg-2017-310
Manuscript under review for journal Biogeosciences
Discussion started: 24 July 2017

Table 1. Summary of the most relevant prescribed parameters in the JSBACH-methane control and reference simulations.

Parameter	Description	Value	Unit
χ_{min_cti}	Threshold to define maximum areas that can be flooded in a grid cell (TOPMODEL)	12	[-]
f	Exponential decay of transmissivity with depth (TOPMODEL)	2.0	[-]
d_r	Root diameter	2	mm
r	Resistance factor of root exodermis	0.8	[-]
h_{exo}	Thickness of exodermis	0.06	mm
R_{fr}	Principal fraction of the pore-free soil volume occupied by roots	40	%
ϕ	Porosity of snow	0.64	[-]
h_{snow}	Snow depth threshold	5	cm
$f_{CH4anox}$	Fraction of anoxic decomposed carbon that becomes CH_4	0.5	[-]
$D_{air}^{CH_4}$	Diffusion coefficient of CH_4 in free air at 0 °C and 1 atm	1.95×10^{-5}	$m^2\ s^{-1}$
$D_{air}^{O_2}$	Diffusion coefficient of O_2 in free air at 0 °C and 1 atm	1.82×10^{-5}	$m^2\ s^{-1}$
ρ_{ice}	Ice density	910	$kg\ m^{-3}$
ρ_{snow}	Snow density (Together with ρ_{ice} leads to: ϕ=0.64 and τ=0.77)	330	$kg\ m^{-3}$

Biogeosciences Discuss., https://doi.org/10.5194/bg-2017-310
Manuscript under review for journal Biogeosciences
Discussion started: 24 July 2017

Table 2. Results from sensitivity experiments (the specific descriptions of the parameters listed below are given in Table 1). Statistical *p*-values are given for the experiments whose results significantly differ from the results in the reference simulation.

Variable	Value	Unit	Annual mean of total CH_4 / (mg CH_4 m^{-2} d^{-1})
χ_{min_cti}	11	[-]	4.2 ± 5.0*
	12§		6.2 ± 7.3
	13		9.2 ± 10.7*
d_r	2§	mm	6.2 ± 7.3
	5		6.2 ± 7.3
	8		6.2 ± 7.3
R_{ff}	0.2	[-]	6.2 ± 7.3
	0.4§		6.2 ± 7.3
	0.6		6.2 ± 7.3
ϕ	0.64§	[-]	6.2 ± 7.3
	0.71		6.2 ± 7.3
	0.86		6.2 ± 7.3
h_{snow}	1	cm	6.2 ± 7.3
	3		6.2 ± 7.3
	5§		6.2 ± 7.3
$f_{CH4anox}$	0.1	[-]	1.2 ± 1.4*
	0.3		3.7 ± 4.3*
	0.5§		6.2 ± 7.3

§parameter value in reference simulation; *significant at $p<0.001$

Biogeosciences Discuss., https://doi.org/10.5194/bg-2017-310
Manuscript under review for journal Biogeosciences
Discussion started: 24 July 2017

Figures

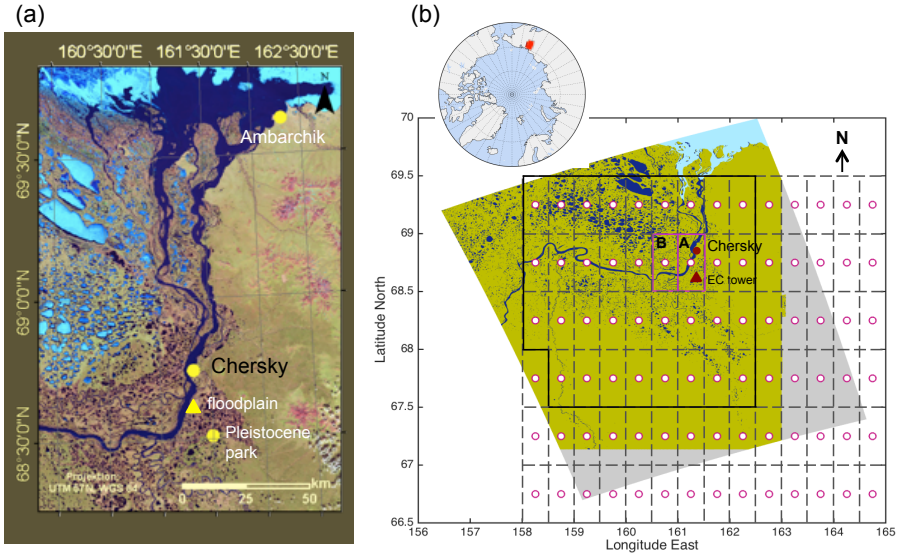

Figure 1 – a) MODIS image showing the heterogeneous landscape in most of the model domain in Northeast Siberia, also showing the location of nearby cities and the floodplain, b) Geographical location of the model domain used in this study also depicted with the midpoints of the model grid cells (pink circles) and boundaries (dashed lines) underlain by a geoTIFF image (data from 01-10 July 2007) from the EAWS product. The boundaries of the grid cells A and B are delimited with pink lines. The 35 model grid cells considered for the validation of modeled inundated areas against the EAWS product are delimited with a continuous dark line.

Biogeosciences Discuss., https://doi.org/10.5194/bg-2017-310
Manuscript under review for journal Biogeosciences
Discussion started: 24 July 2017

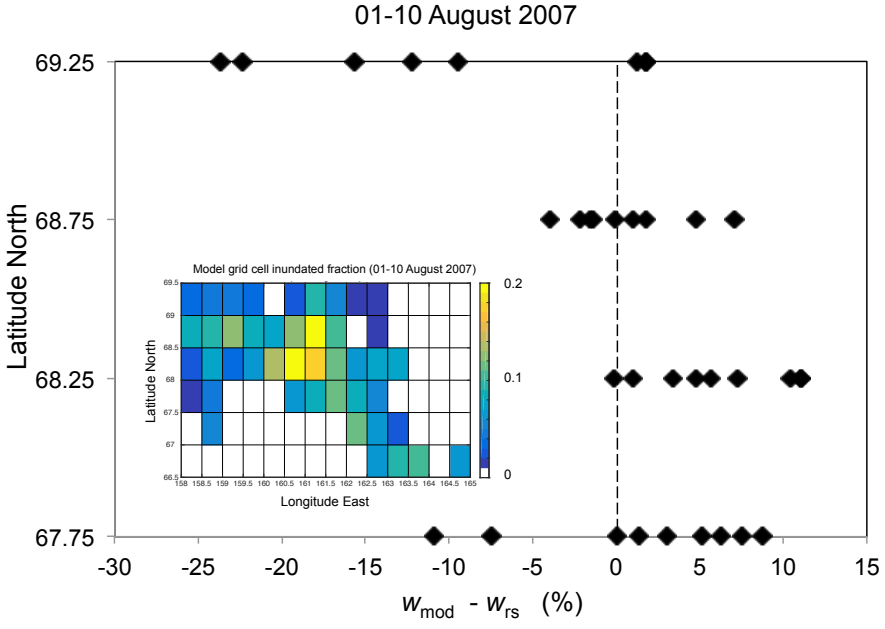

1665 **Figure 2** – Latitudinal distribution of the difference between the fraction of the grid cell inundated areas simulated with TOPMODEL in JSBACH-methane (w_{mod}) and the inundated areas estimated from the EAWS product (w_{rs}) for the same grid cells, for the product from 01-10 August 2007. Inset figure shows the spatial distribution of the fraction of inundated areas in the model domain during 01-10 August 2007. Grid cells with inundated areas < 1 % 1670 are not shown.

Biogeosciences Discuss., https://doi.org/10.5194/bg-2017-310
Manuscript under review for journal Biogeosciences
Discussion started: 24 July 2017

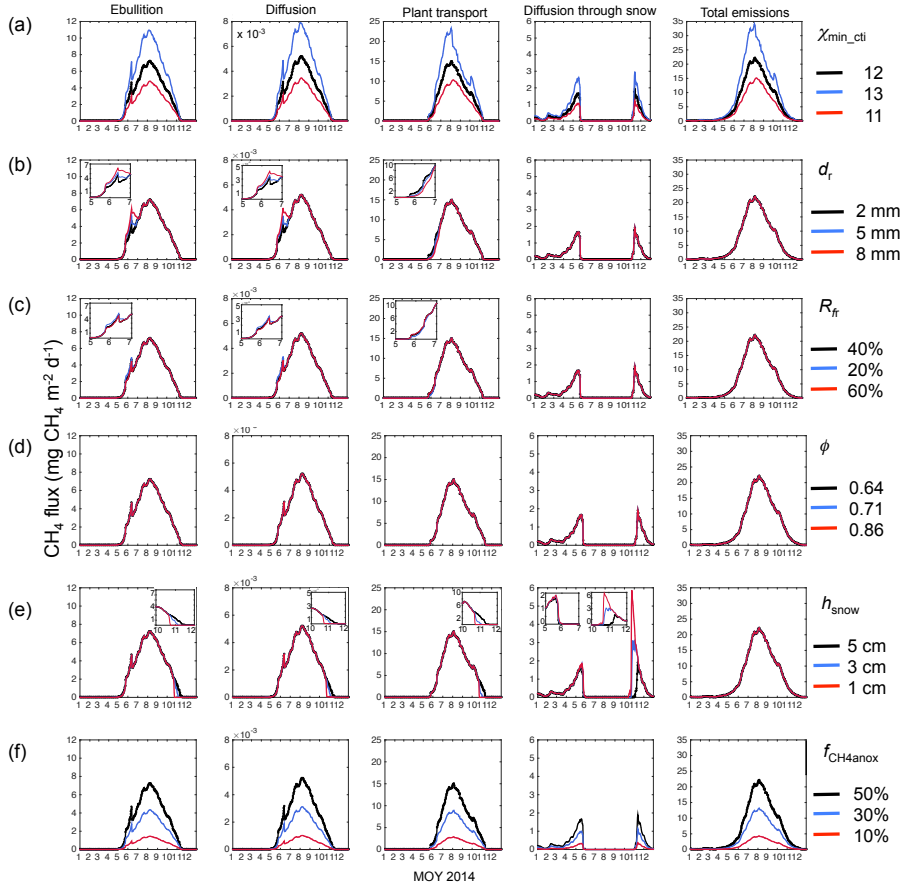

1675 **Figure 3** – Results from the sensitivity experiments for the six selected parameters described in Table 2. Daily methane emissions for the individual transport pathways and total methane emissions are shown.

Biogeosciences Discuss., https://doi.org/10.5194/bg-2017-310
Manuscript under review for journal Biogeosciences
Discussion started: 24 July 2017

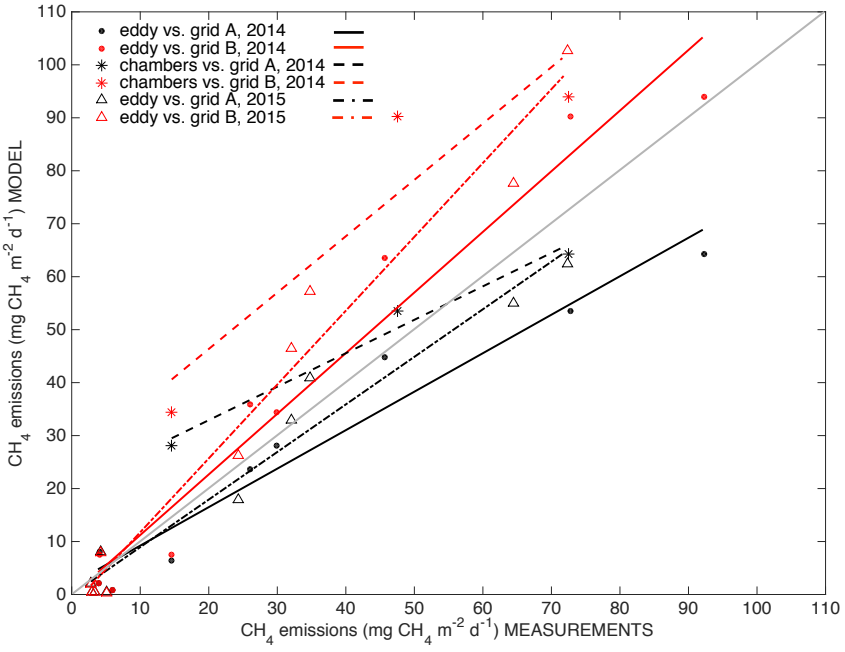

1680

Figure 4 – Comparison between modeled CH_4 emissions and flux measurements by chambers and eddy covariance in the Chersky floodplain: correlation between results for model grid cells A and B and measurements during 2014 and 2015 (the light grey line is the 1:1 line).

1685

Biogeosciences Discuss., https://doi.org/10.5194/bg-2017-310
Manuscript under review for journal Biogeosciences
Discussion started: 24 July 2017

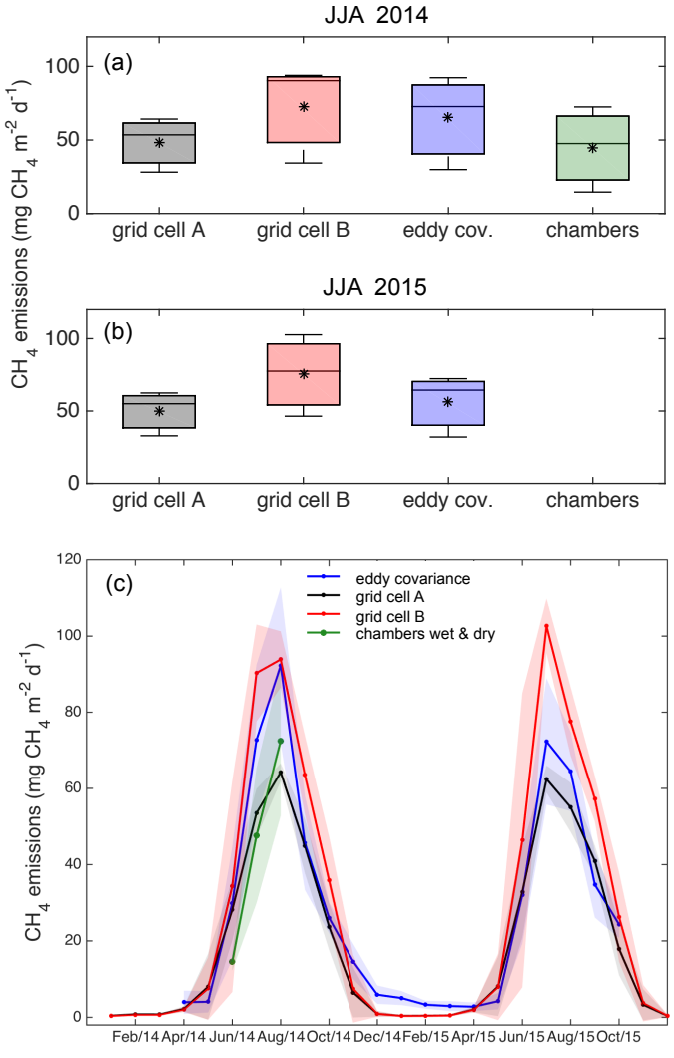

Figure 5 – Box plot for summer (JJA) methane emissions from model grid cells A and B, eddy covariance and chamber flux measurements for a) 2014 and b) 2015 (without chamber flux measurements). The central horizontal line on each box is the median for each data set and whiskers are the minimum and maximum values; c) time series of monthly CH_4 emissions for 2014 and 2015 for grid cells A and B in the model, from eddy covariance as well as chamber flux measurements. Shaded areas depict one standard deviation of the monthly mean of each data set calculated from the daily resolution model output.

Biogeosciences Discuss., https://doi.org/10.5194/bg-2017-310
Manuscript under review for journal Biogeosciences
Discussion started: 24 July 2017

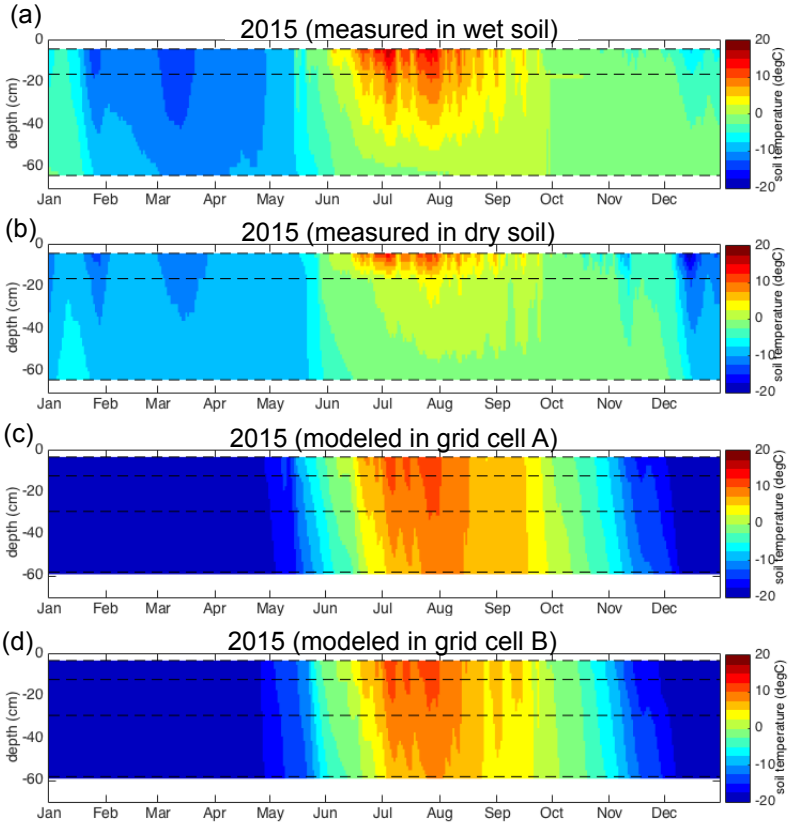

Figure 6 – Hovmöller diagrams showing the time evolution of the vertical profiles of daily soil temperature during 2015 from eddy covariance fluxes measured a) at the wet plot and b) at the dry plot and from the model data c) grid cell A and d) grid cell B. The data were interpolated linearly from the depths where data is available (4, 16 and 64 cm in the sensors of redox systems and 3, 12, 29, and 58 cm in the model).

Biogeosciences Discuss., https://doi.org/10.5194/bg-2017-310
Manuscript under review for journal Biogeosciences
Discussion started: 24 July 2017

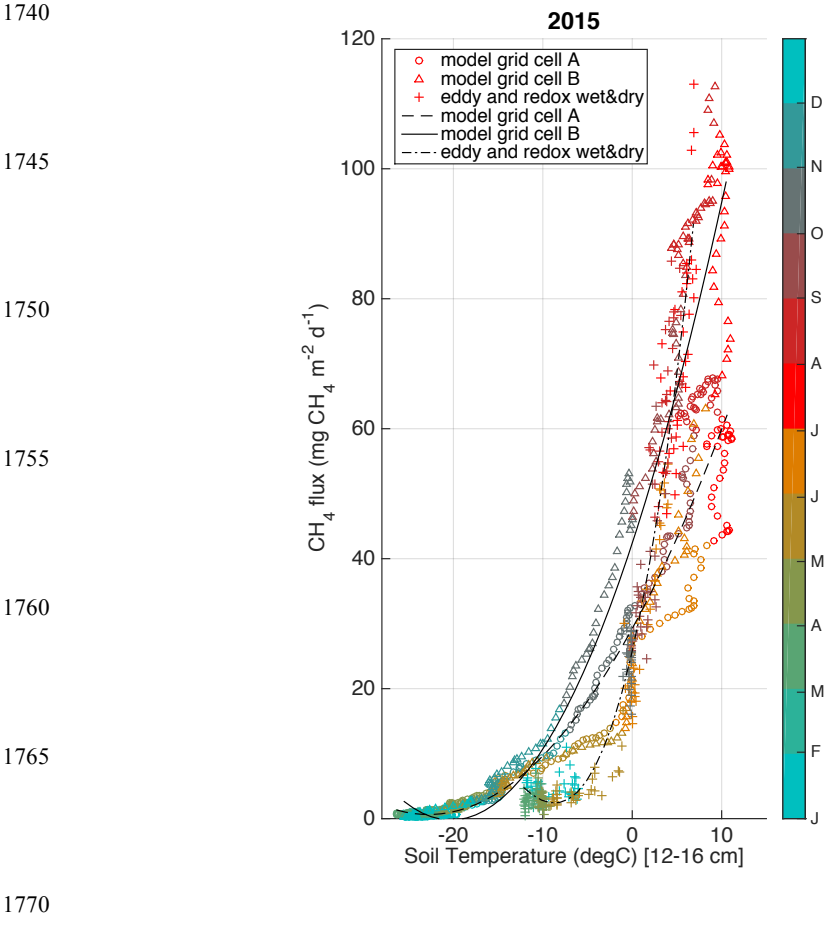

Figure 7 – Model soil temperatures at 12 cm depth and measured values at 16 cm depth (average wet and dry plots) against the total methane emissions for grid cell A and B in 2015.

Biogeosciences Discuss., https://doi.org/10.5194/bg-2017-310
Manuscript under review for journal Biogeosciences
Discussion started: 24 July 2017

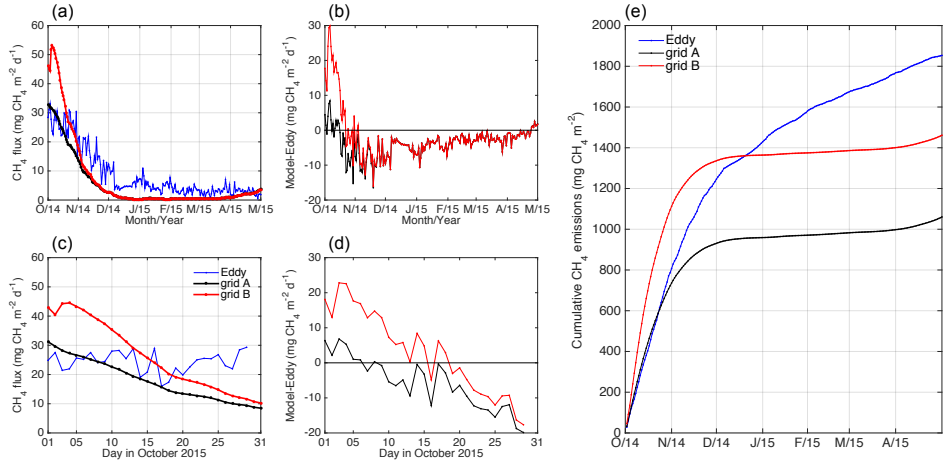

Figure 8 – Time series of the daily mean of methane emissions through snow from eddy covariance measurements and model data for grid cell A and B during: a) October 2014 to March 2015 and c) October 2015; the difference between grid cell A and B, and the eddy covariance data are shown in panels b) and d) for the same period of time; e) cumulative CH_4 emissions for the period from the end of autumn in 2014 until the end of spring in 2015 for the same data sets.

Biogeosciences Discuss., https://doi.org/10.5194/bg-2017-310
Manuscript under review for journal Biogeosciences
Discussion started: 24 July 2017

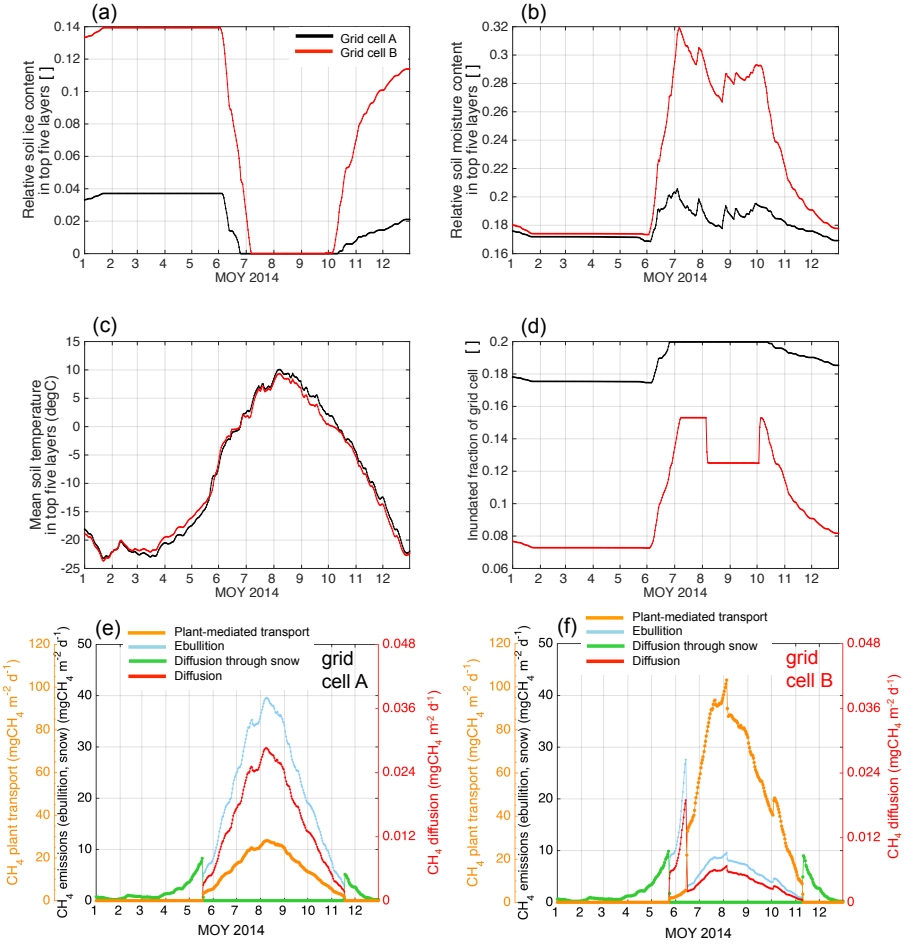

1785

Figure 9 – Time series of mean daily values for ancillary variables and methane emissions via individual pathways for the grid cells A and B during 2014: a) mean relative soil ice content in the top five layers, b) mean relative soil moisture content in the top five layers, c) mean soil temperature in the top five layers, d) inundated fraction of the grid cell, and methane emissions for: e) grid cell A and f) grid cell B.

1790

Biogeosciences Discuss., https://doi.org/10.5194/bg-2017-310
Manuscript under review for journal Biogeosciences
Discussion started: 24 July 2017

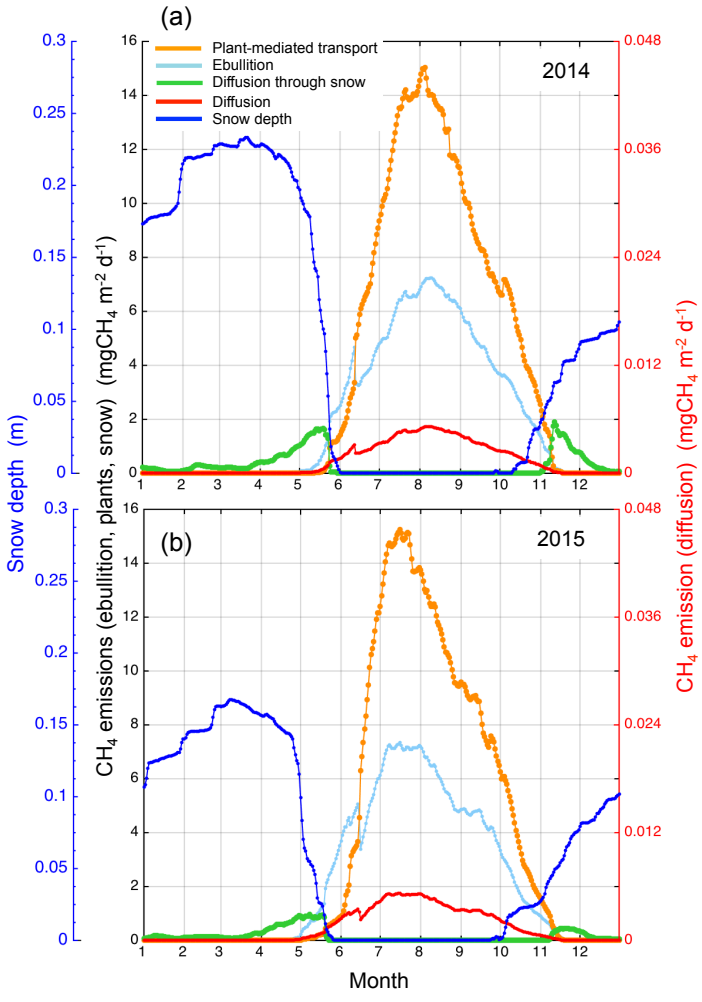

Figure 10 – Year-round mean simulated CH_4 emissions of the model domain through different pathways and domain mean snow depth for a) 2014 and b) 2015.

Biogeosciences Discuss., https://doi.org/10.5194/bg-2017-310
Manuscript under review for journal Biogeosciences
Discussion started: 24 July 2017

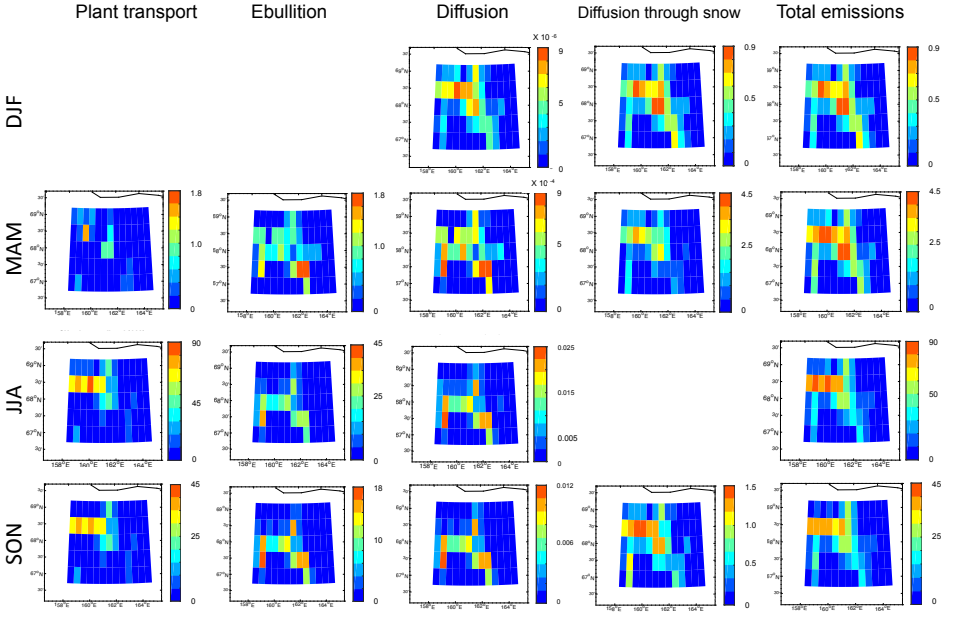

Figure 11 – Spatial distribution of methane emissions due to the individual pathways and the total in the model domain through seasons. Due to the contrastingly different magnitude of emissions between the individual pathways, the color bars are not equal between the figures, thus this figure is only to visually depict the spatial distribution of the emissions within the domain.

Biogeosciences Discuss., https://doi.org/10.5194/bg-2017-310
Manuscript under review for journal Biogeosciences
Discussion started: 24 July 2017

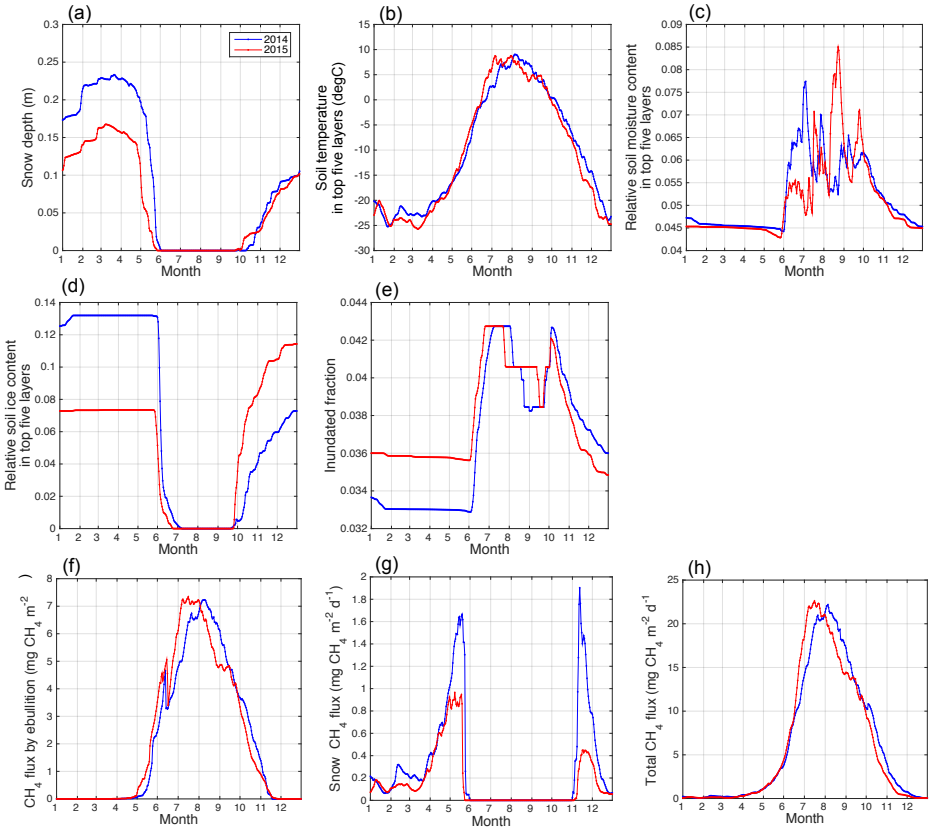

1840 **Figure 12** – Mean daily ancillary variables and CH_4 emissions in the model domain in 2014 and 2015: a) snow depth, b) mean soil temperature in the root zone (top five soil layers), c) domain mean relative soil moisture content in the top five soil layers, d) domain mean relative soil ice content in the top five soil layers, e) inundated fraction of the grid cell, f) CH_4 emissions via ebullition, g) CH_4 emissions through snow and h) total CH_4 emissions.

1845